PROBABILISTIC SEISMIC HAZARD ANALYSIS OF NORTH-EAST INDIA

A Thesis Submitted

in Partial Fulfilment of the Requirements

for the Degree of

MASTER OF TECHNOLOGY

by

Sandip Das

to the

DEPARTMENT OF CIVIL ENGINEERING

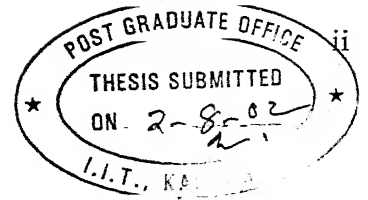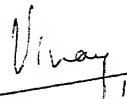# INDIAN INSTITUTE OF TECHNOLOGY KANPUR

August 2002

CERTIFICATE

It is certified that the work contained in the thesis entitled "**Probabilistic Seismic Hazard Analysis of North-East India**" by "**Sandip Das**" has been carried out under my supervision and that this work has not been submitted elsewhere for a degree.

1.8.02

(VINAY KUMAR GUPTA)
Professor
Department of Civil Engineering
Indian Institute of Technology
Kanpur

*dedicated
to
my parents*

ACKNOWLEDGEMENTS

TABLE OF CONTENTS

LIST OF TABLES

LIST OF FIGURES

ABSTRACT

A probabilistic seismic hazard analysis has been carried out for the North-East India. Probabilistic seismic hazard maps have been prepared based on the uniform hazard response spectra for absolute acceleration at stiff rock/rock sites, as those represent a much more complete characterization of seismic hazard than the traditional maps prepared on the basis of peak ground acceleration. For doing the hazard analysis, a new attenuation model based on pseudo-spectral velocity scaling has been proposed by using 261 recorded accelerograms. The entire North-East India has been divided into 0.1° grid size, and the hazard level has been assessed for each node of this grid by considering the seismicity within a 300 km radius area around the node. Using the past earthquake data, the seismicity for the area around each node has been evaluated by defining a and b values of the Gutenberg-Richter recurrence relationship, while taking care of the completeness of the earthquake catalogue. Each node has been considered to be disturbed by 50 annular source elements, for each of which the numbers of events in a magnitude class are estimated by distributing the total number as per the spatial distribution of past earthquake occurrences. Uniform hazard contours for pseudo-spectral acceleration as the hazard parameter have been obtained for a time-interval of 100 years and for 50% confidence level at different time periods for both horizontal and vertical components of ground motion. The trends reflected by these contours validate the seismicity model adopted for this study. Further, a comparison of the estimated hazard levels with those prescribed by the Bureau of Indian Standards code shows that (i) the assumed 50% risk level over 100 years service life in the code is not consistent with the peak ground

acceleration specified for the North-East India, and that (ii) the present practice of specifying seismic hazard through peak ground acceleration and a fixed spectral shape may be inappropriate for structures in most areas of the North-East region.

CHAPTER I

INTRODUCTION

1.1 General Introduction

Seismic hazard analysis plays an important role in earthquake-resistant design of structures by providing a rational value of input hazard parameter. There can be several parameters to characterize the hazard levels and there are different methods to estimate those. The traditional way of characterizing seismic hazard is based on peak ground acceleration (PGA). The main shortcoming of using PGA is however that this cannot provide any information about the duration and frequency content of shaking, which are highly correlated with the damage potential of ground motion. Also, PGA is often found to be poorly correlated with the damage potential of ground motion (Dahle et al. (1990), Musson (2000)), and hence, response parameters such as pseudo-spectral velocity (PSV), pseudo-spectral acceleration (PSA) are increasingly being used as hazard parameters. These parameters are considered to be more comprehensive in describing the hazard levels than PGA.

There are two approaches for estimating the hazard levels: the 'deterministic' approach and the 'probabilistic' approach. Both approaches have their advantages and disadvantages (Reiter (1990)). The deterministic approach is transparent, its input and output parameters are easy to understand (Lindholm and Bungum (2000)), but it does not treat model and data uncertainties. On the other hand, the probabilistic approach correctly reflects the actual knowledge of seismicity (Orozova and Suhadolc (1999)). The scenario earthquake is the central

concept for the 'deterministic' or 'maximum credible earthquake' (MCE) seismic hazard maps (Anderson (1997), Romeo and Prestininzi (2000)). However, when the seismic hazard is influenced by more than one seismic sources, it is impossible to define a single scenario earthquake that is compatible with the results of probabilistic seismic hazard assessment (Bommer et al. (2000)). Moreover, these are not the bigger earthquakes which always influence the hazard levels; smaller events are also important sometimes due to their higher occurrence rates than those for the bigger events (Wheeler and Mueller (2001)). A general rule is that more quantitative the decision to be made is, more appropriate probabilistic hazard and risk assessment would be. Moreover, if many tectonic faults and unidentified seismic sources contribute to the seismic hazard at a site, the integration of those through a probabilistic analysis provides the most useful insight (McGuire (2001)). The essence of probabilistic seismic hazard analysis (PSHA) lies in the uniform hazard spectrum (UHS), which is a convenient tool to compare the hazard representations of different sites (Peruzza et al. (2000)). Since UHS is often the preferred goal of PSHA, any of the spectral properties can be considered as a hazard parameter. Moreover, for the design of important structures, hazard analysis should consider frequency-dependent amplification of ground motion associated with the local site conditions, and in such cases, use of the spectral hazard parameters becomes essential (McGuire et al. (2001)).

PSHA can be carried out in various ways depending on how one defines the model of seismicity. There may be the subjective way (Cornell (1968)) where a subjective judgement is involved in the definition of seismic source zones, or the 'historic' way which requires the past earthquake data only and does not require any specification of source zones (Veneziano et al. (1984)). In this approach, em-

pirical distribution of the seismic hazard parameter is estimated for each of the past events, and then by normalizing this distribution for the duration of seismic event catalogue, the annual rate of exceedance of a specified value of the hazard parameter is obtained. In the present study, however, an objective way making use of the spatial distribution of the past earthquake data is attempted. The major disadvantage of any subjective procedure lies with the requirement of the specification of the seismogenic source zones. Often tectonic provinces or specific active faults are not clearly identified and mapped, and the causes of seismicity are not well understood (Kijko and Öncel (2000)). The main disadvantage of any catalogue-dependent approach of defining seismicity model, on the other hand, is that these do not always work for a region where the seismic event catalogues are likely to be incomplete in a major way (Wheeler and Mueller (2001)). This approach may however be used, when the available data is presumably complete for the last few years, by using the statistical approach of Stepp (1973) to determine the periods in which there is completeness of data for different magnitude ranges.

In the present study, PSHA of North-East India has been carried out. It is based on an objective approach of defining seismicity, since the region is characterized by a very complicated tectonic set-up (Verma et al. (1976)) and because enough past earthquake data is available to meet the requirement. Seismic hazard analysis for a region requires a site-specific attenuation model, based on which ground motion is estimated at a site due to disturbance at the source, for a given level of confidence. In the present case, a spectral attenuation relationship is desirable since the target is to estimate the UHS at various sites of the region. PGA, earthquake intensity or any other single parameter can also be

used as a measure of shaking, and the return period (which is, of course, closely related to the annual probability of exceedance) may be estimated as a function of that parameter (Cornell (1968), Milne and Davenport (1969), Douglas and Ryall (1975)). However, the detailed spectral nature of ground motion is often overlooked in doing so, since a standard spectral shape (a shape which is independent of magnitude, epicentral distance, focal depth, etc.) may be scaled to the parameter considered (Anderson and Trifunac (1977)). For example, larger events are known to be capable of contributing longer period components to the strong shaking, and thus, those lead to broader spectra with relatively larger long-period amplitudes (Trifunac (1978)). The high-frequency waves usually attenuate faster, and therefore, the shape of the response spectrum also depends on source-to-site distance, even when events of equal magnitudes are considered at the same source (Trifunac (1989)). In fact, the dependence of spectral shape on many scaling parameters makes it difficult to represent all possibilities with one standard spectral shape (Trifunac (1992)).

For North-East India, no spectral attenuation relationship is available till date. Hence, an attenuation model based on PSV scaling is developed by using a total of 261 accelerograms from six different earthquake events. There have been a large number of past studies on developing case-specific PSV scaling models, e.g., those by Johnson (1973), McGuire (1978), Cornell et al. (1979), Devillers and Mohammadioun (1981), Joyner and Fumal (1984), Crouse et al. (1988), Atkinson (1990), Dahle et al. (1990), Niazi and Bozorgnia (1992), Tento et al. (1992), Boore et al. (1993), Musson et al. (1994), Theodulidis and Papazachos (1994), Sabetta and Pugliese (1996), Spudich et al. (1999) and Chapman (1999). However, in contrast to the models developed therein, the

proposed model takes care of both horizontal and vertical components of ground motion simultaneously, as in the models of Trifunac (1980), Trifunac and Lee (1989), Lee (1993), Lee and Manić (1994). The entire region of North-East India is covered by considering about 2500 equally-spaced sites, and each of these sites is assumed to be under the hazard of seismic activity within a 300 km radius area around that site. Seismicity in each of these areas is determined by using Gutenberg-Richter (G-R) magnitude-frequency relationship (Gutenberg and Richter (1942)) which is obtained from the knowledge of past earthquake events with epicenters in the area. For obtaining the UHS at a site, Poissonian model of earthquake occurrences is assumed and the probability that a given value of PSV at a time-period will be exceeded is estimated by considering the formulation of Anderson and Trifunac (1977). It is also assumed that each site is surrounded by 50 annular source elements with individual seismicity based on the observed spatial distribution of past earthquake events in that area. With the hazard levels known at various sites in form of UHS for different probabilities of exceedance, seismic hazard maps are obtained in terms of PSA contours for a period of next 100 years and the estimated hazard levels are compared with those prescribed by IS: 1893 (2002).

1.2 Organization

This work is presented in four chapters following this chapter.

In Chapter II, a PSV-based spectral attenuation model is developed for stiff soil/rock sites at North-East India. The validity of this model is checked by comparing the estimated PSV spectra with the actual PSV spectra for a few

recorded accelerograms. A parametric study is also carried out along with the illustrations.

In Chapter III, an objective model of seismicity is proposed for North-East India and G-R relation-based seismicity is defined in about 2500 circular sub-regions on the basis of available earthquake catalogue for this region. For this, the completeness of earthquake catalogue is first checked for different magnitude ranges. In each sub-region, the calculated seismicity is distributed over 50 annular source elements by considering the spatial distribution of past earthquake occurrences.

In Chapter IV, existing formulation for estimating PSV spectra for a specific probability of exceedance in given number of years is briefly reviewed and 5% damping uniform hazard spectra are obtained for various sites and for different probabilities of exceedance. Hazard maps are then generated in terms of PSA contours for the entire region at different time-periods and compared with the codal provisions.

A brief summary and conclusions of this study are presented in Chapter V.

CHAPTER II

ATTENUATION MODEL FOR NORTH-EAST INDIA

2.1 Introduction

A site-specific attenuation model is the key element in any seismic hazard analysis for an area of interest. Since each area has its own geological characteristics, it is essential to develop an empirical attenuation model using the strong motions data previously recorded at several stations in that region. Most attenuation models are based on the scaling for PGA. PGA is however poorly correlated with the damage potential of ground motion. It is also associated with zero time-period response and thus can not provide any information about other time-periods. Therefore a spectral attenuation model based on PSV scaling will be developed in this chapter for North-East India. Such a model will help us in generating a hazard spectrum of a given functional with equal probability of exceedance uniformly at all frequencies.

2.2 Database

To develop the spectral attenuation model for the North-East India, strong motion accelerogram data recorded at several stations in that region has been used. Unfortunately, this data is available at present just for six earthquake events. A total of 261 accelerograms recorded from these earthquake events on stiff soil/rock sites have been used to develop the proposed attenuation model. The details of this database are shown in Table 2.1. At a station, the data for two horizontal components has been combined by applying square-root-of-sum-of-

Table 2.1 - Particulars of the Database

Earthquake Event	Recording Station			Epicentral
	Name	Latitude (degree)	Longitude (degree)	Distance (km)
	Baithalangso	25.97	92.60	60.19
	Dauki	25.20	92.03	46.20
	Khliehriat	25.35	92.37	29.12
Date: September 10, 1986	Nongkhlaw	25.68	91.63	58.43
Focal Depth: 28 km	Nongpoh	25.92	91.88	50.15
Magnitude: 5.5	Nongstoin	25.52	91.27	93.92
Epicenter Latitude: 25.56°	Panimur	25.67	92.80	60.98
Epicenter Longitude: 92.20°	Pynursla	25.30	91.92	42.07
	Saitsama	25.72	92.38	25.05
	Ummulong	25.52	92.17	8.71
	Umsning	25.73	91.88	36.96
	Baithalangso	25.97	92.60	113.98
	Bamungao	25.90	93.02	75.01
	Berlongfer	25.77	93.25	47.41
	Bokajan	26.02	93.77	60.39
Date: May 18, 1987	Diphu	25.92	93.43	51.46
Focal Depth: 50 km	Gunjung	25.32	93.02	63.27
Magnitude: 5.7	Haflong	25.17	93.02	67.89
Epicenter Latitude: 25.48°	Hajadisa	25.38	93.30	32.42
Epicenter Longitude: 93.60°	Hatikhali	25.65	93.12	53.51
	Laisong	25.20	93.32	43.11
	Nongpoh	25.92	91.88	180.03
	Panimur	25.67	92.80	82.36
	Saitsama	25.72	92.38	124.85
	Umrongso	25.52	92.63	98.54
	Baigao	25.40	92.87	140.01
	Baithalangso	25.97	92.60	125.70
	Dauki	25.20	92.03	66.12
	Gunjung	25.32	93.02	156.22
	Haflong	25.17	93.02	160.67
	Hatikhali	25.65	93.12	165.51
Date: February 6, 1988	Katakhal	24.83	92.63	140.16
Focal Depth: 15 km	Khliehriat	25.35	92.37	92.59
Magnitude: 5.8	Mawphlang	25.47	91.77	31.32
Epicenter Latitude: 25.50°	Nongkhlaw	25.68	91.63	26.76
Epicenter Longitude: 91.46°	Nongpoh	25.92	91.88	60.42
	Pynursla	25.30	91.92	49.47
	Saitsama	25.72	92.38	95.77
	Shillong	25.57	91.90	44.53
	Ummulong	25.52	92.17	69.28
	Umrongso	25.52	92.63	116.17
	Umsning	25.73	91.88	49.76

Table 2.1 (continued)

Earthquake Event	Station Name	Latitude	Longitude	Distance
	Baigao	25.40	92.87	168.71
	Baithalangso	25.97	92.60	204.38
	Bamungao	25.90	93.02	163.34
	Berlongfer	25.77	93.25	135.38
	Bokajan	26.02	93.77	102.74
	Cherrapunji	25.27	91.73	281.23
	Dauki	25.20	92.03	253.38
	Diphu	25.92	93.43	125.06
	Doloo	24.92	92.78	182.96
	Gunjung	25.32	93.02	153.91
	Hajadisa	25.38	93.30	123.50
Date: August 6, 1988	Harengajao	25.12	92.87	171.63
Focal Depth: 91 km	Hojai	26.00	92.85	181.38
Magnitude: 7.2	Jellalpur	25.00	92.47	213.21
Epicenter Latitude: 25.38°	Jhirighat	24.80	93.12	157.59
Epicenter Longitude: 94.53°	Kalain	24.98	92.58	202.52
	Katakhal	24.83	92.63	200.67
	Khliehriat	25.35	92.37	217.26
	Koomber	24.95	93.02	161.03
	Mawphlang	25.47	91.77	277.61
	Panimur	25.67	92.80	176.22
	Pynursla	25.30	91.92	264.32
	Saitsama	25.72	92.38	218.78
	Shillong	25.57	91.90	264.80
	Silchar	24.83	92.80	184.81
	Ummulong	25.52	92.17	239.38
	Umrongso	25.52	92.63	192.54
	Umsning	25.73	91.88	268.68
	Bamungao	25.90	93.02	259.06
	Berlongfer	25.77	93.25	230.72
Date: January 10, 1990	Diphu	25.92	93.43	224.04
Focal Depth: 119 km	Gunjung	25.32	93.02	234.45
Magnitude: 6.1	Hajadisa	25.38	93.30	207.69
Epicenter Latitude: 24.75°	Hojai	26.00	92.85	277.73
Epicenter Longitude: 95.24°	Laisong	25.20	93.32	202.31
	Maibang	25.30	93.13	221.51
	Panimur	25.67	92.80	266.09
	Umrongso	25.52	92.63	277.85
	Baigao	25.40	92.87	252.66
Date: May 6, 1995	Bamungao	25.90	93.02	253.31
Focal Depth: 122 km	Berlongfer	25.77	93.25	226.54
Magnitude: 6.4	Diphu	25.92	93.43	216.93
Epicenter Latitude: 25.01°	Hatikhali	25.65	93.12	234.49
Epicenter Longitude: 95.34°	Hojai	26.00	92.85	273.30
	Umrongso	25.52	92.63	278.78

squares (SRSS) combination on the PSV spectra for the two components. As the ground motion at a site has strong azimuthal dependence, the SRSS combination helps to normalize for that dependence. The so-obtained PSV spectra should be divided by $\sqrt{2}$ to get the normalized spectra for each horizontal component separately. Thus, a total of 174 PSV spectra (including SRSS-combined spectra for horizontal component) have been used for finding the attenuation model. The damping ratio considered for these computations is 5 percent. The maximum value of time-period for which the spectra have been computed is 1.0 s, as the data is contaminated by base-line distortions and low-frequency noise signals, and may not therefore give reliable spectra values for the longer time-periods.

2.3 Model Selection

Prior to performing the regression analysis on the PSV data, it is required to select a functional form of attenuation model which comprises the parameters governing the attenuation of ground shaking. To select the best attenuation model, one has to try several empirical models, and by regression analysis for each of those, one can decide on the appropriateness of that model with respect to the existing database, though all such attenuation models are theoretically possible. The appropriateness of a particular model can be evaluated based on a few criteria. First, the regression coefficients obtained from the regression analysis for the model have to be physically meaningful. If this criterion is not satisfied, the model has to be rejected. Next, the model should fit into the data with as little errors as possible. Further, the model should also be able to generate reasonable spectra for a wider range of input parameters, beyond those covered in the input data.

To develop a scaling model that can predict the PSV spectra, earthquake magnitude and distance of source/epicenter to site should be considered as the major controlling parameters. Further, to develop a model for both horizontal and vertical motions, another controlling parameter, v, has to be considered where v can be taken equal to 0 for horizontal motions and 1 for vertical motions (Trifunac (1980), Trifunac and Lee (1989)). One may consider either epicentral distance or hypocentral distance. For a region where there is not much variation in the focal depths of various events, one can go for epicentral distance while ignoring the focal depths. However, in North-East India, the average focal depth of events ranges from 10 to 100 km. Hence, the model should take care of both epicentral distance and focal depth. This can be done either by considering hypocentral distance as the distance parameter or by separately considering epicentral distance and focal depth as controlling parameters. Both possibilities will be considered in the present study.

Despite a considerable amount of work on spectral attenuation relationship in the last three decades, only the models proposed by Trifunac (1980), Trifunac and Lee (1989), Lee (1993), Lee and Manić (1994) and Lee (1995) take care of both horizontal and vertical motions simultaneously. The functional forms of these models however are such that those require more information about input parameters than what are available in the present situation, e.g., shear wave velocity, depth of sediment deposits. Hence, a new functional form needs to be developed.

Let the following model be first considered:

$$\log[PSV(T)] = c_1(T) + c_2(T)M + c_3(T)M^2 + c_4(T)\Delta + c_5(T)\log(\Delta) + c_6(T)v \quad (2.1)$$

where, M is the earthquake magnitude, Δ is the hypocentral distance, and T is the time-period of single-degree-of-freedom (SDOF) oscillator. This model comprises all possible governing parameters except for those corresponding to amplification related to local soil conditions. The term, $c_3(T)M^2$, takes care of saturation at higher magnitude level. The term, $c_4(T)\Delta$, takes care of attenuation due to absorption, while the term, $c_5(T)\log(\Delta)$, takes care of attenuation due to geometrical spreading. After regression analysis based on this model, the values of $c_4(T)$ are obtained to be positive numbers, much against their usual values between -0.0002 to -0.002 (Dahle et al. (1990)). This implies that the data considered in this study is not good enough to properly account for the absorption phenomenon. Moreover, upto a distance of 300 km, the effect of anelastic spreading is not that significant as compared to geometrical spreading (Dahle et al. (1990)). On dropping the term, $c_4(T)\Delta$, the next model is considered to be

$$\log[PSV(T)] = c_1(T) + c_2(T)M + c_3(T)M^2 + c_4(T)\log(\Delta) + c_5(T)v \qquad (2.2)$$

In this model, $c_3(T)$ takes care of the saturation at higher value of magnitude, and theoretically, it should be negative and much smaller than $c_2(T)$ in magnitude while $c_2(T)$ should always be positive (Trifunac and Lee (1989)). After regression analysis, however, the values of calculated coefficients exhibit these trends only at high frequencies. This leads to the following alternative based on separating the roles of epicentral distance and focal depth,

$$\log[PSV(T)] = c_1(T) + c_2(T)M + c_3(T)M^2 + c_4(T)\log(R) + c_5(T)\log(h) + c_6(T)v$$
$$(2.3)$$

where, R is epicentral distance and h is the focal depth. This model fails to give proper values of $c_2(T)$ and $c_3(T)$ at long periods, and thus, the available data

appears to be too limited to account for saturation and absorption. On dropping the term involving M^2 in Eq. (2.2), following alternative model is considered:

$$\log[PSV(T)] = c_1(T) + c_2(T)M + c_3(T)\log(\Delta) + c_4(T)v \qquad (2.4)$$

This model gives reasonable values of regression coefficients, and hence, is suitable for describing the spectral attenuation in the North-East India region. This however does not differentiate between two cases of identical distances and different focal depths, and therefore, an extra term involving focal depth is introduced (Crouse et al. (1988)). The proposed model therefore becomes

$$\log[PSV(T)] = c_1(T) + c_2(T)M + c_3(T)h + c_4(T)\log(\sqrt{R^2 + h^2}) + c_5(T)v \quad (2.5)$$

without any loss in reasonableness of regression coefficients.

2.4 Regression Analysis

The regression analysis is performed in two stages to get the values of regression coefficients. In the first stage, $c_4(T)$ and $c_5(T)$ are estimated by performing linear regression analysis on the following model,

$$\log[PSV(T)] = \sum_{i=1}^{n} a_i e_j + c_4(T)\log(\sqrt{R^2 + h^2}) + c_5(T)v \qquad (2.6)$$

where, $e_j = 1$ for the jth earthquake event and zero otherwise, and $n = 6$ (total number of events). Through this step, the coefficients, $c_4(T)$ and $c_5(T)$, are decoupled from the other three coefficients. In the second stage, the remaining coefficients are determined by performing the linear regression analysis for the equation,

$$\log[PSV(T)] - c_4'(T)\log(\sqrt{R^2 + h^2}) - c_5'(T)v = c_1(T) + c_2(T)M + c_3(T)h \quad (2.7)$$

where, $c_4'(T)$ and $c_5'(T)$ are obtained from the first stage of regression analysis.

2.5 Results and Discussion

(i) *Regression Coefficients and Error Spectra*

Fig. 2.1 shows the estimated (smoothed) coefficients, $c_1'(T)$, $c_2'(T)$, $c_3'(T)$, $c_4'(T)$ and $c_5'(T)$. In Table 2.2, these values are tabulated at 51 time-periods. It is observed from Fig. 2.1 that the value of $c_3'(T)$, which reflects the possible effects of focal depth for fixed hypocentral distance, is positive and significant at higher frequencies, and becomes insignificant at longer periods. This is expected since the deeper earthquakes are supposed to produce more high-frequency body-wave motion than shallower earthquakes of the same magnitude and hypocentral distance due to less anelastic attenuation and greater stress drop (McGarr (1984)). By using the estimated regression coefficients, the estimated value of $\log[PSV(T)]$ becomes

$$\log[PSV'(T)] = c_1'(T) + c_2'(T)M + c_3'(T)h + c_4'(T)\log(\sqrt{R^2 + h^2}) + c_5'(T)v \quad (2.8)$$

With $PSV(T)$ representing actual values of PSV spectra for an accelerogram, the residuals $\epsilon(T)$ are calculated as

$$\epsilon(T) = \log[PSV(T)] - \log[PSV'(T)] \qquad (2.9)$$

for all 174 PSV spectra.

For the actual probability $p(\epsilon, T)$ that the residual spectrum, $\epsilon(T)$ (see Eq. (2.9)), will not be exceeded, Fig. 2.2 shows the plots of the residual spectra corresponding to $p(\epsilon, T) = 0.1$ (10%) to 0.9 (90%) for 5% damping PSV data. There are nine sets of curves, from bottom to the top of the figure, corresponding
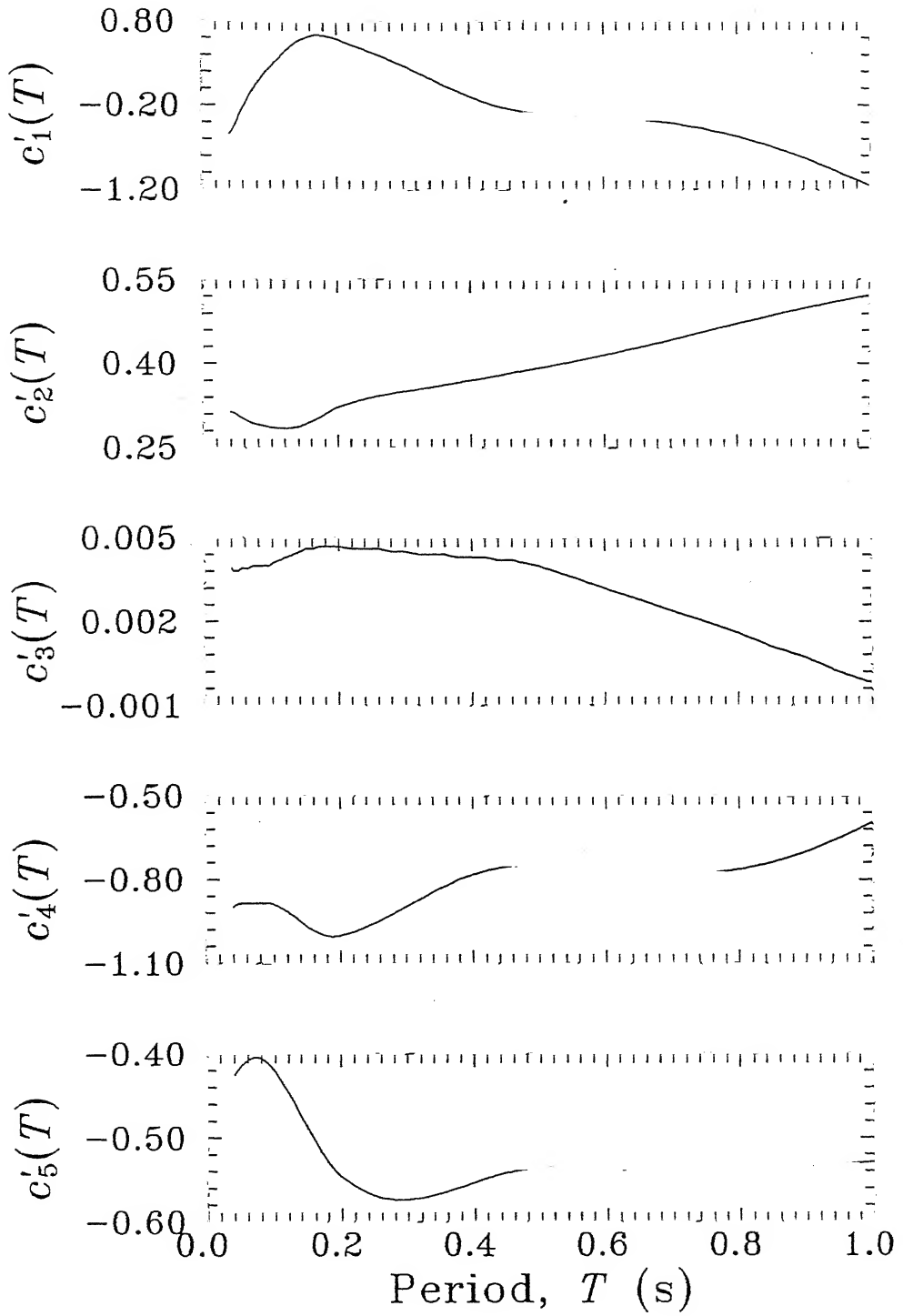
Figure 2.1 Variation of Estimated (Smoothed) Regression Coefficients with T.

Table 2.2 - Estimated (Smoothed) Regression Coefficients

| Period, T	$c_1'(T)$	$c_2'(T)$	$c_3'(T)$	$c_4'(T)$	$c_5'(T)$
0.040	-0.5402	0.3140	0.0039	-0.9001	-0.4251
0.042	-0.5156	0.3133	0.0038	-0.8959	-0.4230
0.044	-0.4889	0.3123	0.0038	-0.8923	-0.4208
0.046	-0.4596	0.3111	0.0038	-0.8893	-0.4186
0.048	-0.4277	0.3097	0.0038	-0.8873	-0.4164
0.050	-0.3937	0.3081	0.0038	-0.8862	-0.4146
0.055	-0.3065	0.3042	0.0039	-0.8854	-0.4107
0.060	-0.2211	0.3006	0.0039	-0.8853	-0.4076
0.065	-0.1401	0.2974	0.0039	-0.8854	-0.4055
0.070	-0.0655	0.2948	0.0040	-0.8854	-0.4044
0.075	0.0016	0.2928	0.0040	-0.8851	-0.4045
0.080	0.0614	0.2913	0.0040	-0.8845	-0.4057
0.085	0.1150	0.2900	0.0040	-0.8839	-0.4080
0.090	0.1643	0.2889	0.0040	-0.8839	-0.4113
0.095	0.2108	0.2878	0.0040	-0.8854	-0.4157
0.100	0.2557	0.2868	0.0041	-0.8892	-0.4211
0.110	0.3427	0.2852	0.0042	-0.9009	-0.4334
0.120	0.4251	0.2844	0.0043	-0.9155	-0.4467
0.130	0.4989	0.2849	0.0044	-0.9326	-0.4607
0.140	0.5602	0.2872	0.0045	-0.9508	-0.4751
0.150	0.6054	0.2912	0.0046	-0.9684	-0.4896
0.160	0.6328	0.2967	0.0046	-0.9837	-0.5037
0.170	0.6426	0.3033	0.0047	-0.9951	-0.5170
0.180	0.6374	0.3101	0.0047	-1.0019	-0.5288
0.190	0.6206	0.3165	0.0047	-1.0038	-0.5388
0.200	0.5957	0.3217	0.0047	-1.0006	-0.5464
0.220	0.5375	0.3301	0.0046	-0.9870	-0.5578
0.240	0.4757	0.3368	0.0046	-0.9689	-0.5662
0.260	0.4110	0.3421	0.0046	-0.9472	-0.5716
0.280	0.3431	0.3462	0.0045	-0.9227	-0.5741
0.300	0.2716	0.3498	0.0045	-0.8965	-0.5741
0.320	0.1971	0.3533	0.0044	-0.8700	-0.5721
0.340	0.1208	0.3569	0.0044	-0.8444	-0.5685
0.360	0.0446	0.3608	0.0044	-0.8207	-0.5639
0.380	-0.0291	0.3650	0.0043	-0.7998	-0.5586
0.400	-0.0975	0.3693	0.0043	-0.7821	-0.5531
0.420	-0.1583	0.3738	0.0043	-0.7682	-0.5479
0.440	-0.2091	0.3782	0.0042	-0.7581	-0.5432
0.460	-0.2484	0.3826	0.0042	-0.7519	-0.5396
0.480	-0.2755	0.3869	0.0041	-0.7495	-0.5373
0.500	-0.2913	0.3912	0.0040	-0.7505	-0.5364
0.550	-0.3147	0.4025	0.0036	-0.7582	-0.5365
0.600	-0.3369	0.4145	0.0032	-0.7672	-0.5375
0.650	-0.3662	0.4276	0.0028	-0.7753	-0.5387
0.700	-0.4101	0.4418	0.0024	-0.7797	-0.5397
0.750	-0.4748	0.4565	0.0020	-0.7770	-0.5400
0.800	-0.5644	0.4712	0.0016	-0.7640	-0.5393
0.850	-0.6807	0.4854	0.0011	-0.7384	-0.5378
0.900	-0.8217	0.4986	0.0007	-0.6998	-0.5353
0.950	-0.9821	0.5108	0.0002	-0.6507	-0.5321
1.000	-1.1532	0.5225	-0.0002	-0.5955	-0.5285
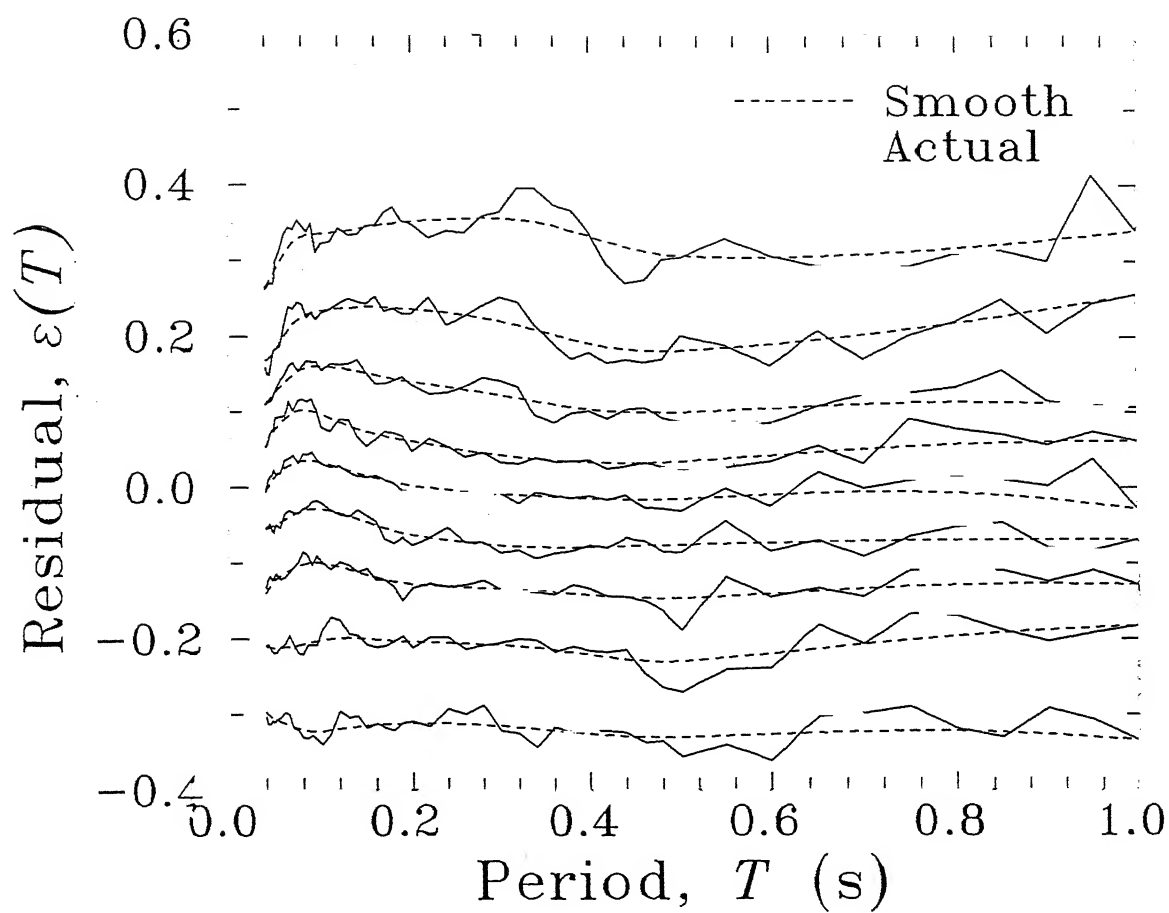
Figure 2.2 Residual Spectra for Different Values of p.

to the probability levels of 0.1 through 0.9. In each set, the zig-zag solid line represents the actual residuals while the smooth dashed line represents their smoothed values, with smoothing having been done along the time-period axis. The smoothed values of $\epsilon(p, T)$ are tabulated in Table 2.3 for the nine different values of p.

If $\epsilon(p, T)$ represents the error level for probability, p, and time-period, T, the PSV spectra for desired level of confidence may be estimated from

$$\log[PSV'(p, T)] = c_1'(T) + c_2'(T)M + c_3'(T)h + c_4'(T)\log(\sqrt{R^2 + h^2})$$
$$+ c_5'(T)v + \epsilon(p, T) \qquad (2.10)$$

(ii) *Estimated PSV Spectra*

Figs. 2.3(a) and 2.3(b) show comparison between the PSV spectra computed from the recorded accelerograms, for a small and shallow event (May 18, 1987) with $M = 5.7$, $h = 50$ km, with the PSV spectra estimated by using Eq. (2.10). Fig. 2.3(a) shows the comparison for horizontal spectrum recorded at a station (Hatikhali) with $R = 53.51$ km, while Fig. 2.3(b) shows the comparison for vertical spectrum recorded at a station (Berlongfer) with $R = 47.41$ km. In each figure, the pair of top ($p = 0.9$) and bottom ($p = 0.1$) estimated PSV curves (see the solid lines) outlines the 80% confidence interval of the predicted amplitudes, while the dashed line corresponds to the actual spectrum.

Figs. 2.4(a) and 2.4(b) show the comparison for a large and deep event (August 6, 1988) with $M = 7.2$, $h = 91$ km. Fig. 2.4(a) shows the comparison for horizontal spectrum recorded at a station (Hajadisa) with $R = 123.50$ km, while Fig. 2.4(b) shows the comparison for vertical spectrum recorded at a station

Table 2.3 - Smoothed Residual Spectra, $\epsilon(p, T)$, for Different Values of Probability Level, p

| Period, T (s)	Probability Level, p								
	0.1	0.2	0.3	0.4	0.5	0.6	0.7	0.8	0.9
0.040	-0.2964	-0.2098	-0.1391	-0.0541	-0.0054	0.0555	0.1115	0.1687	0.2645
0.042	-0.2994	-0.2106	-0.1342	-0.0533	0.0001	0.0607	0.1142	0.1700	0.2687
0.044	-0.3020	-0.2112	-0.1299	-0.0524	0.0052	0.0657	0.1170	0.1718	0.2731
0.046	-0.3041	-0.2116	-0.1262	-0.0514	0.0095	0.0702	0.1200	0.1743	0.2777
0.048	-0.3057	-0.2118	-0.1232	-0.0503	0.0131	0.0743	0.1229	0.1775	0.2823
0.050	-0.3069	-0.2118	-0.1209	-0.0490	0.0159	0.0776	0.1258	0.1813	0.2869
0.055	-0.3093	-0.2114	-0.1164	-0.0455	0.0213	0.0847	0.1328	0.1910	0.2979
0.060	-0.3115	-0.2108	-0.1125	-0.0421	0.0259	0.0908	0.1393	0.2004	0.3079
0.065	-0.3138	-0.2101	-0.1090	-0.0387	0.0296	0.0957	0.1451	0.2088	0.3165
0.070	-0.3160	-0.2092	-0.1060	-0.0356	0.0324	0.0994	0.1500	0.2160	0.3233
0.075	-0.3182	-0.2081	-0.1034	-0.0329	0.0344	0.1017	0.1540	0.2216	0.3283
0.080	-0.3201	-0.2069	-0.1014	-0.0307	0.0356	0.1028	0.1570	0.2258	0.3315
0.085	-0.3216	-0.2055	-0.1000	-0.0291	0.0360	0.1027	0.1590	0.2288	0.3334
0.090	-0.3225	-0.2040	-0.0992	-0.0282	0.0358	0.1016	0.1603	0.2309	0.3344
0.095	-0.3227	-0.2026	-0.0992	-0.0280	0.0349	0.0997	0.1609	0.2324	0.3349
0.100	-0.3223	-0.2015	-0.0998	-0.0285	0.0336	0.0974	0.1608	0.2336	0.3353
0.110	-0.3207	-0.1998	-0.1019	-0.0307	0.0303	0.0923	0.1599	0.2354	0.3364
0.120	-0.3188	-0.1987	-0.1046	-0.0336	0.0267	0.0872	0.1584	0.2369	0.3379
0.130	-0.3170	-0.1983	-0.1076	-0.0371	0.0231	0.0824	0.1565	0.2381	0.3398
0.140	-0.3154	-0.1985	-0.1109	-0.0409	0.0196	0.0782	0.1542	0.2389	0.3420
0.150	-0.3141	-0.1992	-0.1144	-0.0450	0.0162	0.0745	0.1518	0.2392	0.3443
0.160	-0.3132	-0.2001	-0.1177	-0.0491	0.0129	0.0713	0.1492	0.2391	0.3465
0.170	-0.3125	-0.2010	-0.1208	-0.0530	0.0100	0.0685	0.1467	0.2387	0.3484
0.180	-0.3120	-0.2019	-0.1234	-0.0565	0.0073	0.0660	0.1444	0.2380	0.3500
0.190	-0.3116	-0.2026	-0.1255	-0.0595	0.0050	0.0638	0.1423	0.2371	0.3512
0.200	-0.3114	-0.2030	-0.1269	-0.0618	0.0032	0.0617	0.1405	0.2362	0.3521
0.220	-0.3112	-0.2038	-0.1288	-0.0655	0.0001	0.0576	0.1372	0.2342	0.3537
0.240	-0.3114	-0.2045	-0.1302	-0.0687	-0.0025	0.0536	0.1339	0.2318	0.3551
0.260	-0.3121	-0.2053	-0.1313	-0.0714	-0.0048	0.0499	0.1305	0.2289	0.3562
0.280	-0.3133	-0.2063	-0.1323	-0.0737	-0.0066	0.0465	0.1268	0.2251	0.3568
0.300	-0.3150	-0.2076	-0.1333	-0.0756	-0.0082	0.0435	0.1229	0.2205	0.3565
0.320	-0.3170	-0.2093	-0.1345	-0.0770	-0.0095	0.0408	0.1188	0.2151	0.3548
0.340	-0.3192	-0.2115	-0.1359	-0.0780	-0.0108	0.0385	0.1147	0.2090	0.3515
0.360	-0.3214	-0.2142	-0.1375	-0.0784	-0.0119	0.0367	0.1108	0.2026	0.3465
0.380	-0.3236	-0.2173	-0.1393	-0.0784	-0.0130	0.0352	0.1074	0.1965	0.3400
0.400	-0.3256	-0.2207	-0.1412	-0.0781	-0.0140	0.0340	0.1045	0.1910	0.3327
0.420	-0.3273	-0.2240	-0.1431	-0.0775	-0.0148	0.0333	0.1022	0.1866	0.3252
0.440	-0.3287	-0.2269	-0.1446	-0.0768	-0.0154	0.0329	0.1007	0.1834	0.3184
0.460	-0.3296	-0.2290	-0.1457	-0.0760	-0.0155	0.0331	0.1000	0.1816	0.3128
0.480	-0.3300	-0.2297	-0.1460	-0.0754	-0.0152	0.0338	0.0999	0.1811	0.3089
0.500	-0.3297	-0.2290	-0.1456	-0.0748	-0.0144	0.0350	0.1005	0.1818	0.3069
0.550	-0.3280	-0.2246	-0.1429	-0.0734	-0.0116	0.0390	0.1030	0.1856	0.3051
0.600	-0.3259	-0.2190	-0.1397	-0.0722	-0.0088	0.0433	0.1059	0.1904	0.3051
0.650	-0.3238	-0.2128	-0.1362	-0.0710	-0.0064	0.0476	0.1088	0.1962	0.3064
0.700	-0.3222	-0.2064	-0.1328	-0.0699	-0.0049	0.0518	0.1114	0.2028	0.3089
0.750	-0.3213	-0.2006	-0.1300	-0.0690	-0.0048	0.0554	0.1133	0.2102	0.3124
0.800	-0.3216	-0.1954	-0.1279	-0.0684	-0.0063	0.0583	0.1142	0.2183	0.3167
0.850	-0.3232	-0.1911	-0.1267	-0.0680	-0.0096	0.0603	0.1139	0.2271	0.3217
0.900	-0.3260	-0.1877	-0.1265	-0.0679	-0.0146	0.0616	0.1125	0.2364	0.3272
0.950	-0.3297	-0.1848	-0.1270	-0.0680	-0.0209	0.0622	0.1101	0.2460	0.3331
1.000	-0.3339	-0.1823	-0.1278	-0.0681	-0.0279	0.0624	0.1072	0.2558	0.3392
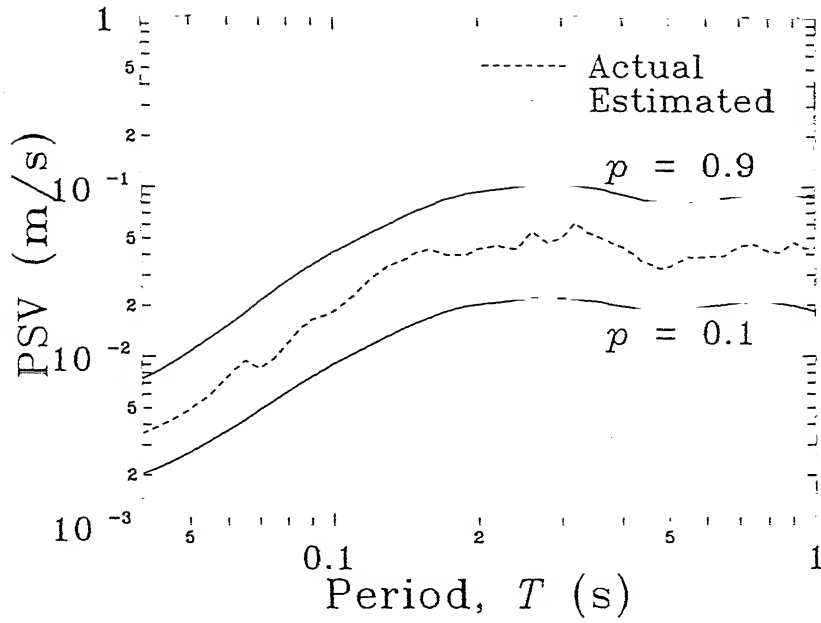
Figure 2.3(a) Comparison of Actual and Estimated PSV Spectra for Hatikhali Record.
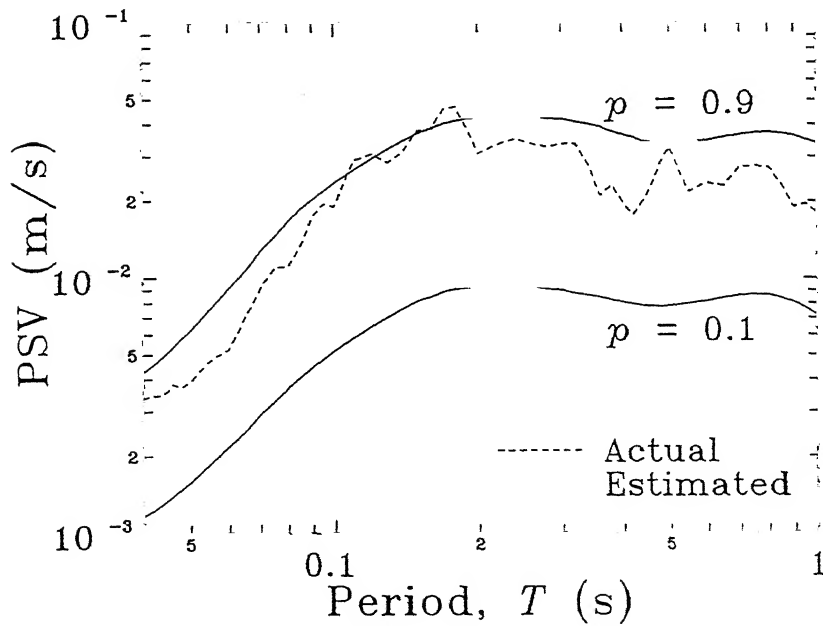

Figure 2.3(b) Comparison of Actual and Estimated PSV Spectra for Berlongfer Record.
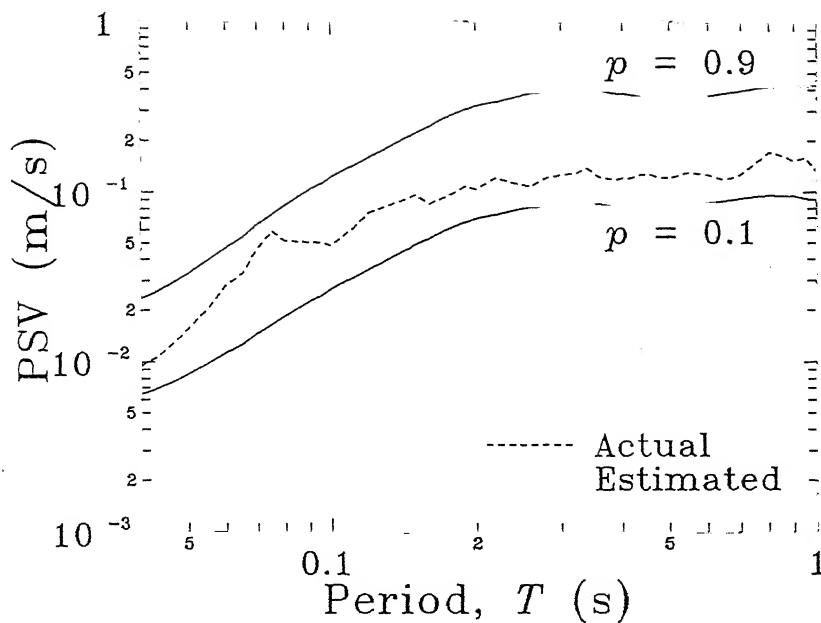
Figure 2.4(a) Comparison of Actual and Estimated PSV Spectra for Hajadisa Record.
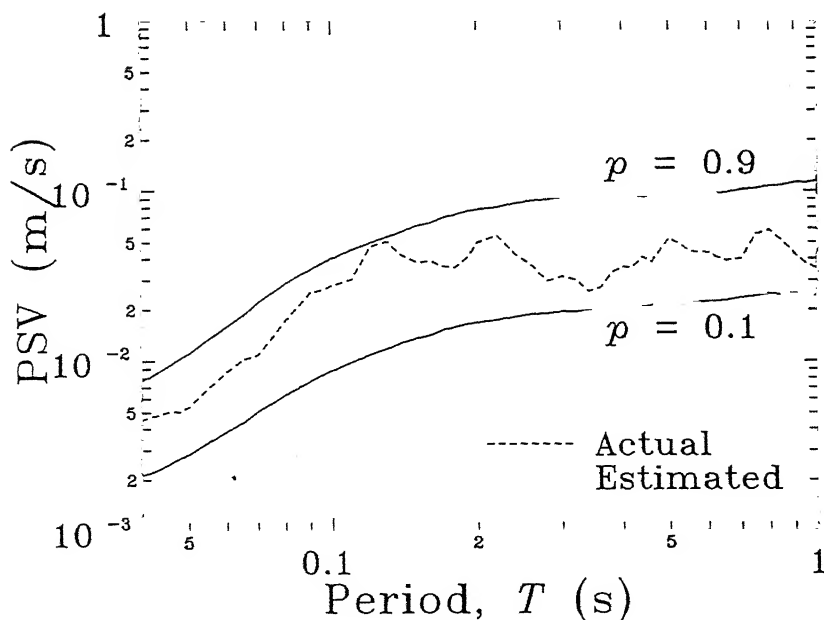

Figure 2.4(b) Comparison of Actual and Estimated PSV Spectra for Gunjung Record.

(Gunjung) with $R = 153.91$ km.

It is clear from the above four figures that the proposed model works well both for shallower and deeper, and smaller and larger events. It also works for near-source and distant sites. However, the 80% confidence band is wide enough to reflect a considerable amount of scattering in the scaling parameter. This highlights the level of uncertainty which comes from the attenuation model alone in a probabilistic seismic hazard analysis.

Figs. 2.5(a) to 2.5(c) show plots for 50% probability PSV spectra for parametric variations respectively in focal depth, epicentral distance and magnitude with other parameter remaining fixed. Fig. 2.5(a) shows the effect of focal depth for $M = 6.5$ and $R = 25$ km. Fig. 2.5(b) shows illustrations of $PSV(T)$ for different epicentral distances, with $M = 6.5$, $h = 25$ km, while Fig. 2.5(c) shows PSV spectra for different magnitudes, with $R = 100$ km, $h = 50$ km. In each figure, the curves without symbols correspond to horizontal motions ($v = 0$), while those with symbols correspond to vertical motions ($v = 1$).

Figs. 2.6(a) and 2.6(b) show how PSV spectrum at $T = 0.2$, 0.4 and 1.0 s attenuates with hypocentral distance for $M = 6.0$, $h = 20$ km. Fig. 2.6(a) shows this for horizontal ground motions, while Fig. 2.6(b) shows this for vertical ground motions. These figures support the well-known fact that the shorter waves attenuate faster than the longer waves.
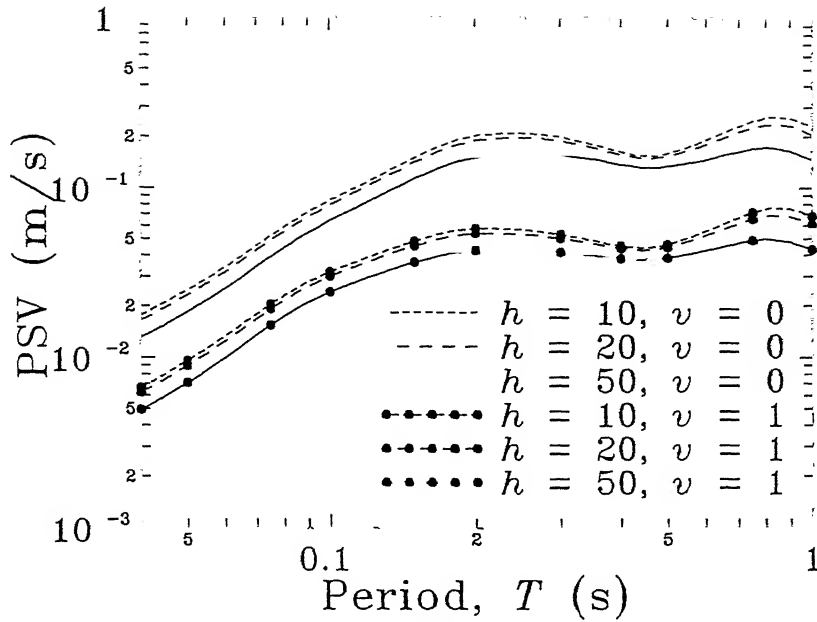
Figure 2.5(a) Comparison of Estimated PSV Spectra for
Different Values of Focal Depth in Case of
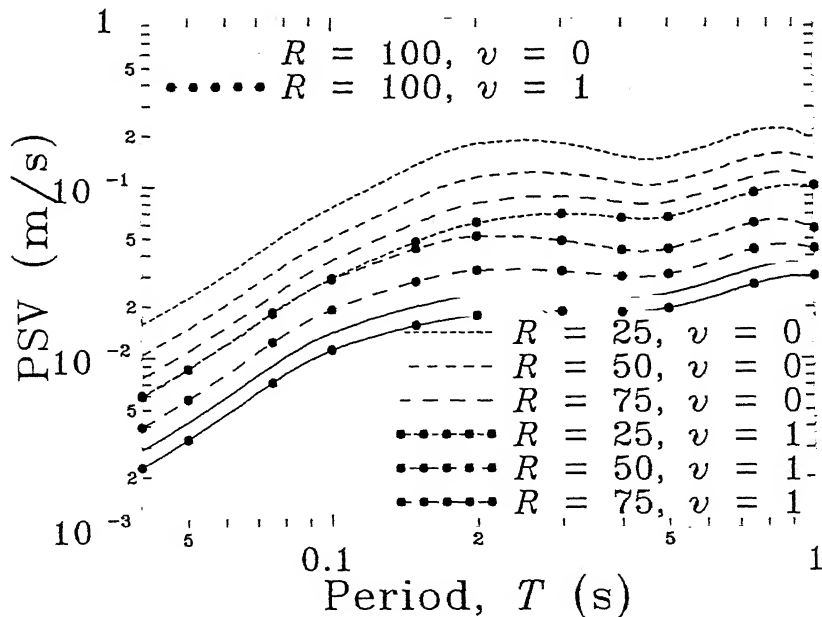$M = 6.5$, $R = 25$ km, $p = 0.5$, and $v = 0,1$.

Figure 2.5(b) Comparison of Estimated PSV Spectra for
Different Values of Epicentral Distance in
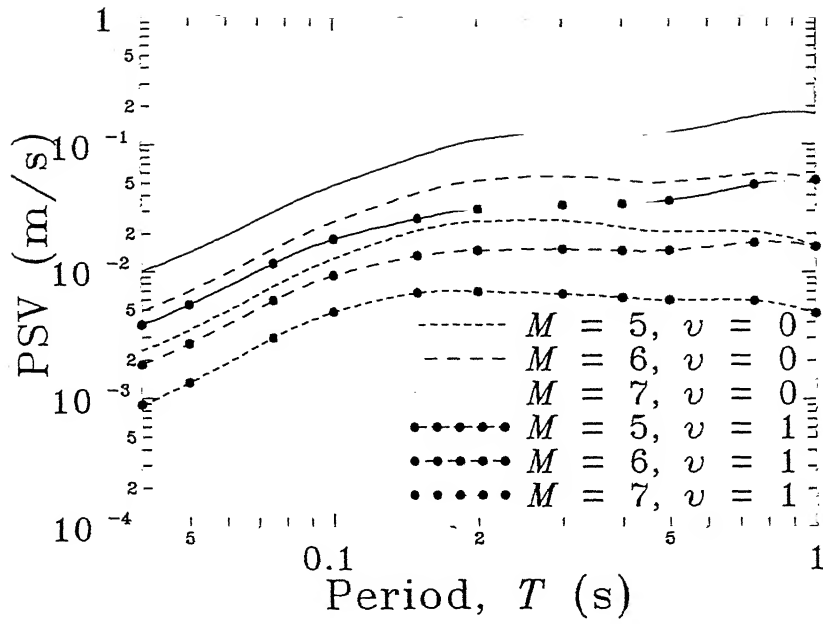Case of $M = 6.5$, $h = 25$ km, $p = 0.5$, and v
$= 0,1$.

Figure 2.5(c) Comparison of Estimated PSV Spectra for Different Values of Magnitude in Case of $R = 100$ km, $h = 50$ km, $p = 0.5$, and $v = 0,1$.
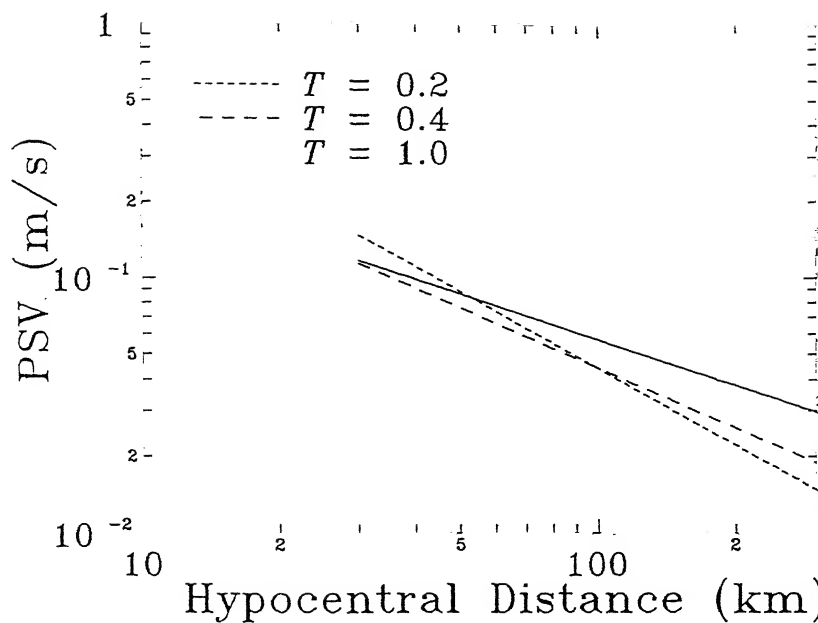
Figure 2.6(a) Variations of PSV Values with Hypocentral Distance at Different Values of T in Case of $v = 0$.
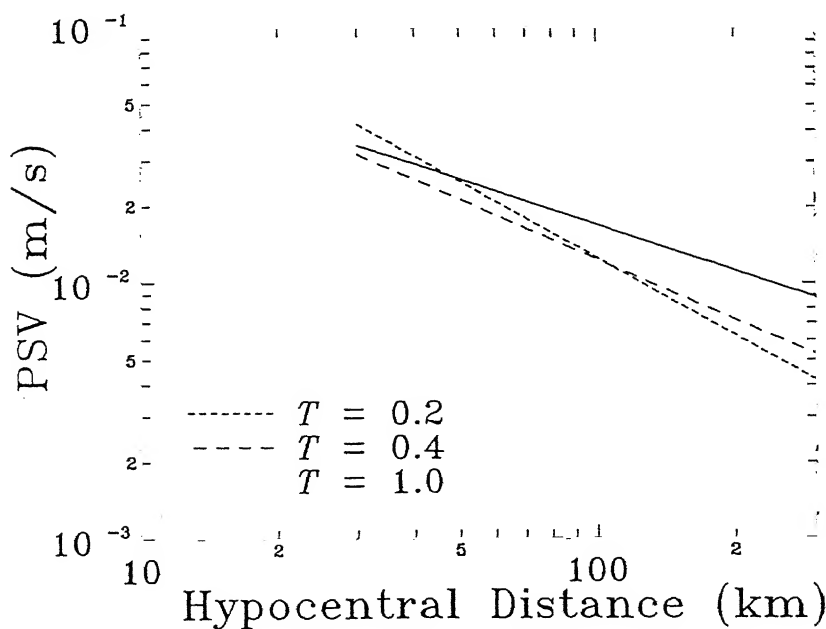
Figure 2.6(b) Variations of PSV Values with Hypocentral Distance at Different Values of T in Case of $v = 1$.

CHAPTER III
SEISMICITY OF NORTH-EAST INDIA

3.1 Introduction

For probabilistic seismic hazard analysis, it is necessary to define the seismicity of the region of interest. The term, seismicity, refers to the expected rates of occurrence of earthquakes in different magnitude ranges. The most popular way to define the seismicity is to specify the two constants in the Gutenberg-Richter (G-R) recurrence relationship for various source zones (Cornell (1968), Orozova and Suhadolc (1999), Kijko and Öncel (2000), Sokolov et al. (2001), Chandler et al. (2001), Kayabali (2002)). This is usually done by using the past earthquake data and/or tectonic features of the region. This study makes use of past earthquake data only, since this data is available for a sufficiently long period of time. For a region like North-East India, which is characterized by very complicated tectonic set-up (Verma et al. (1976)), there may be several different ways to identify the seismic sources. It may thus be difficult to select any of these models, as all of those may be justified by different hypotheses and arguments (Gupta and Ramkrishna (1984)). Therefore, in the present study, an objective approach has been attempted to define the seismicity based only on the knowledge of the spatial distribution of the past earthquakes. Such a model-independence will however reflect the seismicity properly only if the data is available for a sufficiently long period of time. Moreover, the completeness of earthquake catalogue for different magnitude classes has to be checked in such a case (Wheeler and Mueller (2001)). In this chapter, it will be briefly discussed how the completeness of data is checked for this study and how the constants in

the G-R relationship are obtained for different source zones.

3.2 Completeness of Data

Prior to estimating constants in the G-R relationship for any single source zone, it is of crucial importance to check the completeness of earthquake data corresponding to different ranges of magnitude, particularly since the evaluation of seismicity here is entirely based on the past earthquake data. It is obvious that smaller earthquake events occur more frequently than the bigger ones, and hence the recurrence rates of smaller earthquakes can be evaluated even from the most recent data of last 15–20 years in seismically active regions. On the other hand, for bigger events one may have to consider much longer time frame, say that of about 100 years. This raises the possibility of incompleteness of data, due to which, the recurrence rate may be underestimated for smaller events and overestimated for larger events.

To minimize the effect of incompleteness, an empirical and statistically simple method based on the stability of the magnitude recurrence rate is adopted here (Stepp (1973)). According to this method, the entire catalogue of earthquake events is grouped into magnitude ranges, say $\Delta M = 0.4$ for lower magnitude levels and larger for higher magnitude levels, for different time windows, say 5–10 years long for smaller events and 30 years long for bigger events (since bigger events are more rare). The average number of events per year, $R(M)$, are then evaluated in case of each magnitude range for different time windows of increasing lengths, starting with the most recent window. If the first window consists of last five years, the next few windows would consist of the last 10, 15, ... years.

The so-obtained series of $R(M)$ will be analyzed to give the smallest length of the time window for which $R(M)$ becomes stationary. This series must however be long enough so as to include those intervals in which the data is incompletely reported. This minimizes the error of estimation of the mean rate of occurrence; but a certain degree of engineering judgement is required.

The smallest window for which $R(M)$ becomes stationary for a magnitude class represents the minimum period in which complete reporting may be assumed to have taken place. To find this, $R(M)$ is modelled as a Poisson point process in time (Stepp (1973)), such that for a window length of L years, the standard deviation of $R(M)$ is given by

$$S_R = \sqrt{\frac{R(M)}{L}} \tag{3.1}$$

For stationary $R(M)$, S_R is supposed to vary as $\sqrt{1/L}$ with L. The plot of S_R as a function of L, known as the 'completeness plot', indeed shows such behaviour until certain window length, known as the period of completeness, L_C. Figs. 3.1(a)-3.1(g) show the plots of S_R versus L for different magnitude ranges. In each figure, period, L_C, is identified by a distinct departure of the S_R values from a line with $\sqrt{1/L}$ slope. This period is found to be successively longer with each higher magnitude class.

3.3 Gutenberg-Richter Relationship

The evaluation of seismicity is normally carried out by using magnitude-frequency relationship. For a given source zone, the occurrence rate, $N(M)$, of earthquakes with magnitudes greater than or equal to M satisfies the G-R
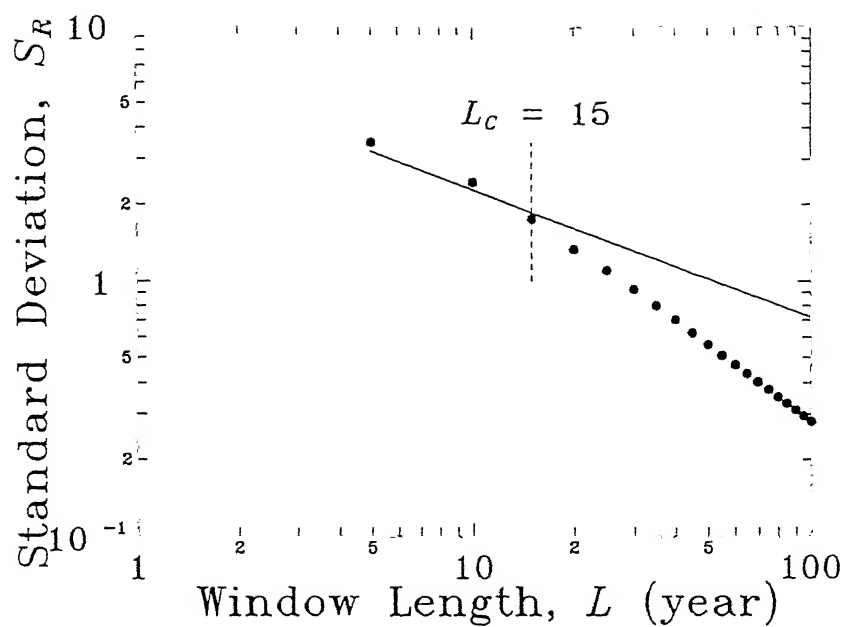
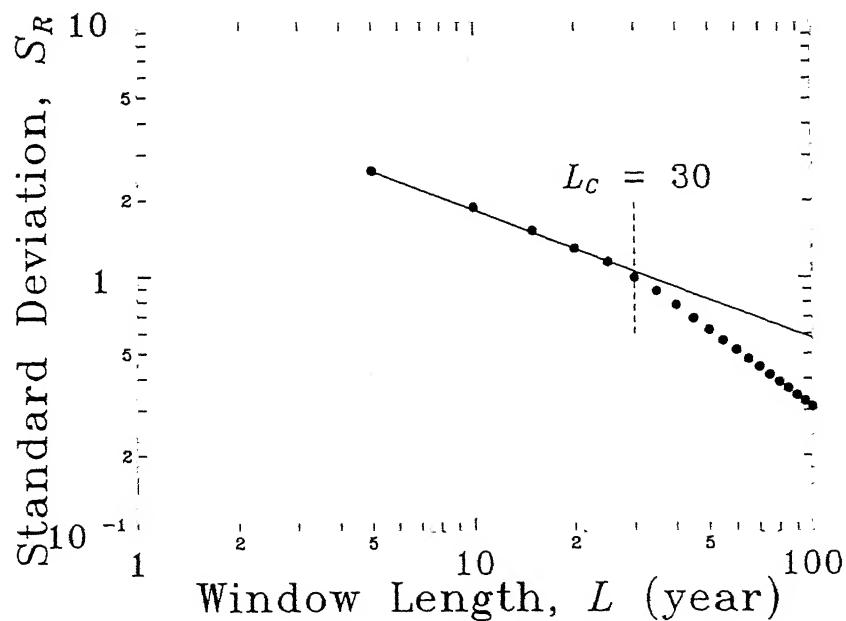**Figure 3.1(a)** Completeness Plot for Magnitude Range, 4.0–4.5.

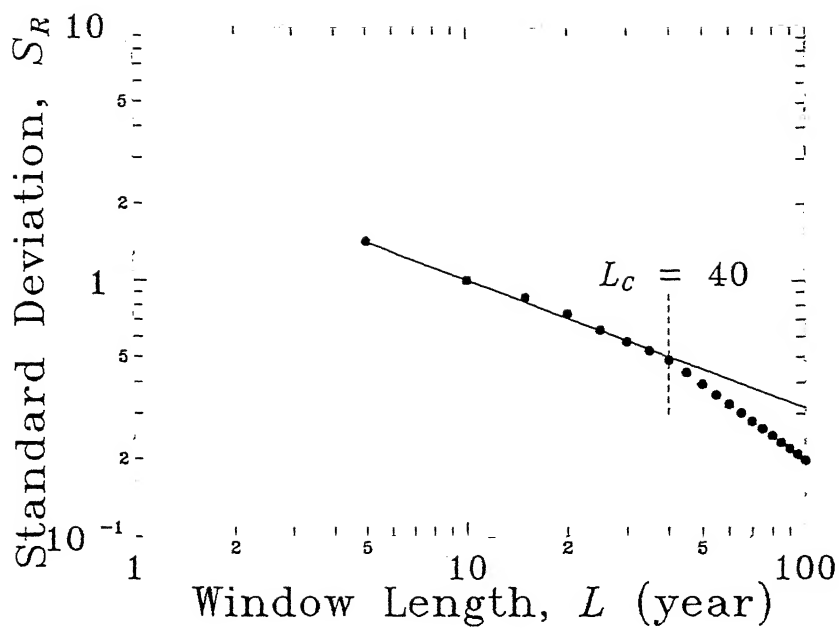**Figure 3.1(b)** Completeness Plot for Magnitude Range, 4.5–5.0.

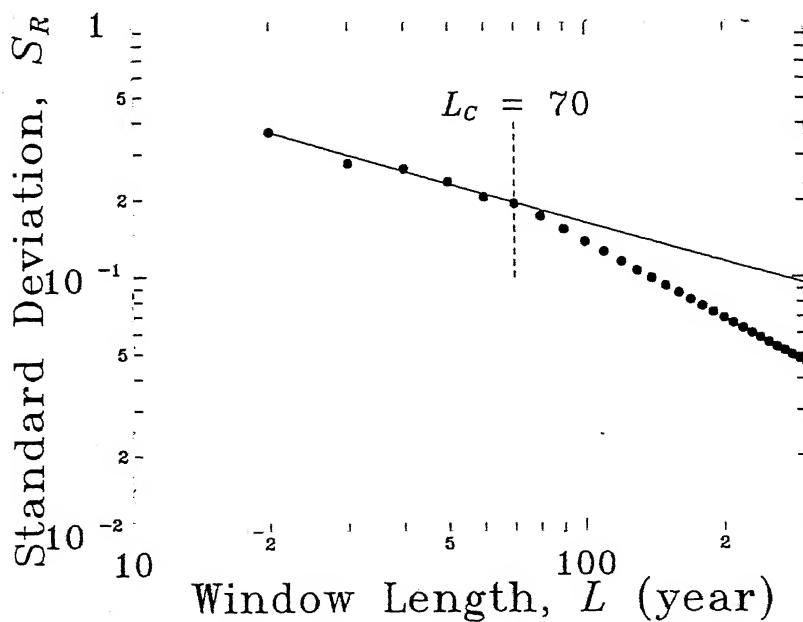**Figure 3.1(c)** Completeness Plot for Magnitude Range, 5.0–5.5.

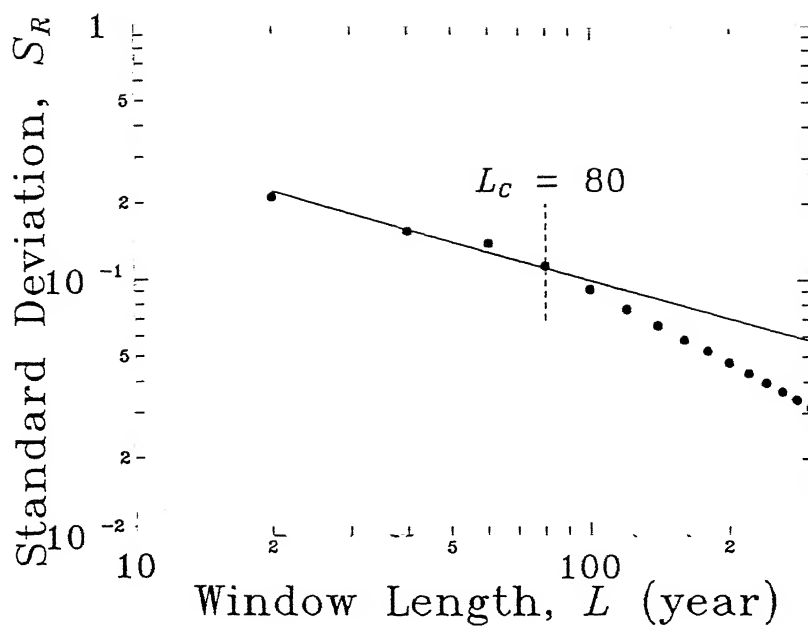**Figure 3.1(d)** Completeness Plot for Magnitude Range, 5.5–6.0.

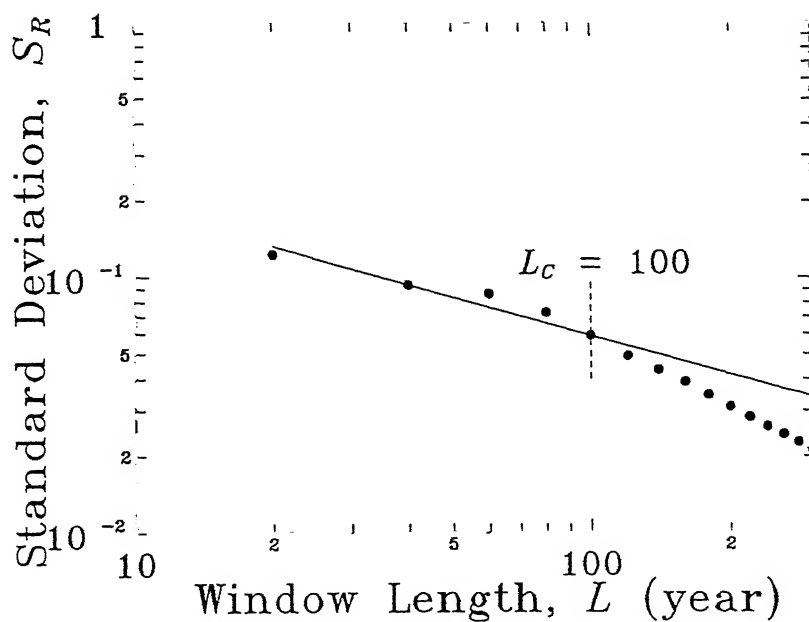**Figure 3.1(e)** Completeness Plot for Magnitude Range, 6.0–6.5.

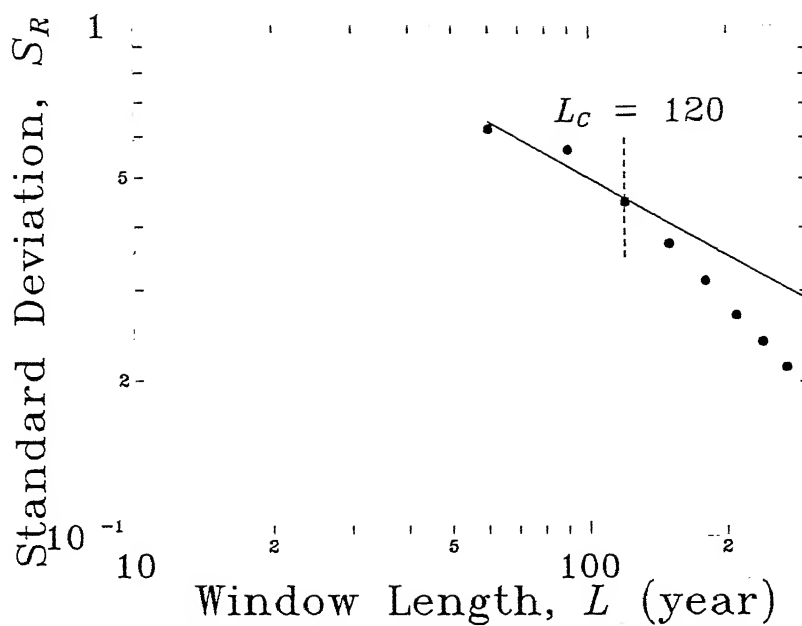**Figure 3.1(f)** Completeness Plot for Magnitude Range, 6.5–7.0.

Figure 3.1(g) Completeness Plot for Magnitude Range, 7.0–8.5.

relationship (Gutenberg and Richter (1942))

$$\log N(M) = a - bM \tag{3.2}$$

where, a and b are constants, determined from the past seismicity data by regression analysis. In this study, the entire North-East India area is sub-divided into a $0.1°$ latitude and $0.1°$ longitude grid, and each intersection point of the grid is considered to be a site which is also assumed to be the centre of a circular zone of 300 km radius. To determine the a and b values for each of these zones, all past events (in the respective periods of completeness) with epicenters in the zone are considered, and the values of $N(M)$, normalized to one-year duration, are determined for different values of magnitude from 4.0 to 8.4. Fitting a straight line to the data points leads to the values of a and b, for example, as shown in Fig. 3.2 for the grid point having $24.4°$ latitude and $94.2°$ longitude. Once a and b are known for a particular circular zone, the number of earthquakes, $N(M)$, with magnitudes between M_j - $\delta M/2$ and $M_j + \delta M/2$ can be obtained from

$$N(M_j) = N\left(M_j - \frac{\delta M}{2}\right) - N\left(M_j + \frac{\delta M}{2}\right) \tag{3.3}$$

To complete the description of seismicity, it is necessary to specify how the earthquake events with number as in Eq. (3.3) are spatially distributed. For this purpose, it is assumed that the 300 km radius circular zone is sub-divided into 50 annular elements with each element acting as a source element at an epicentral distance of $(R_i + R_{i-1})/2$ where R_i, $i = 1, 2, \ldots 50$, is the outer radius of the ith element. The radii, R_1, R_2, $\ldots R_{50}$ are considered to be equally-spaced on logarithmic scale from 1 to 300 km. Further, it is assumed that $N(M_j)$ (see Eq. (3.3)) would be distributed on 50 source elements in the
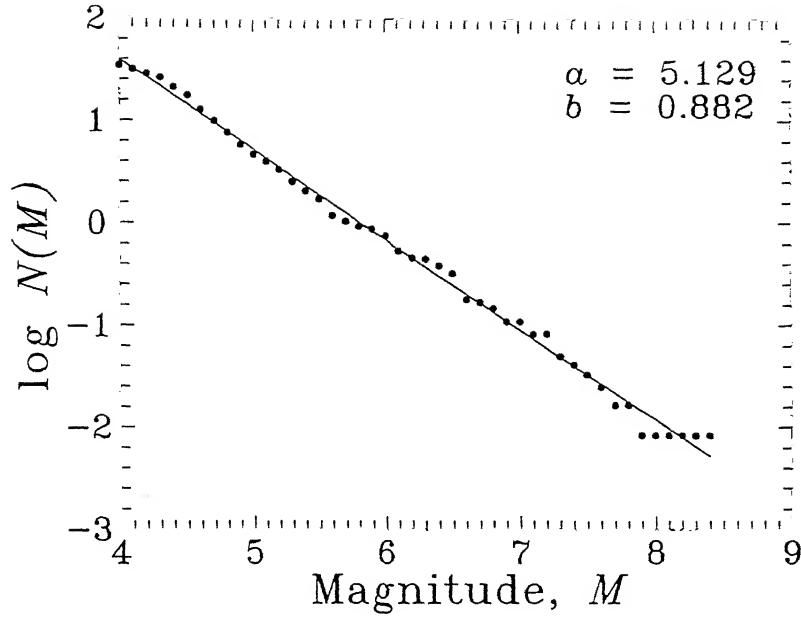
Figure 3.2 Fitting of G-R Relationship to Observed Variation of $\log N(M)$ with M.
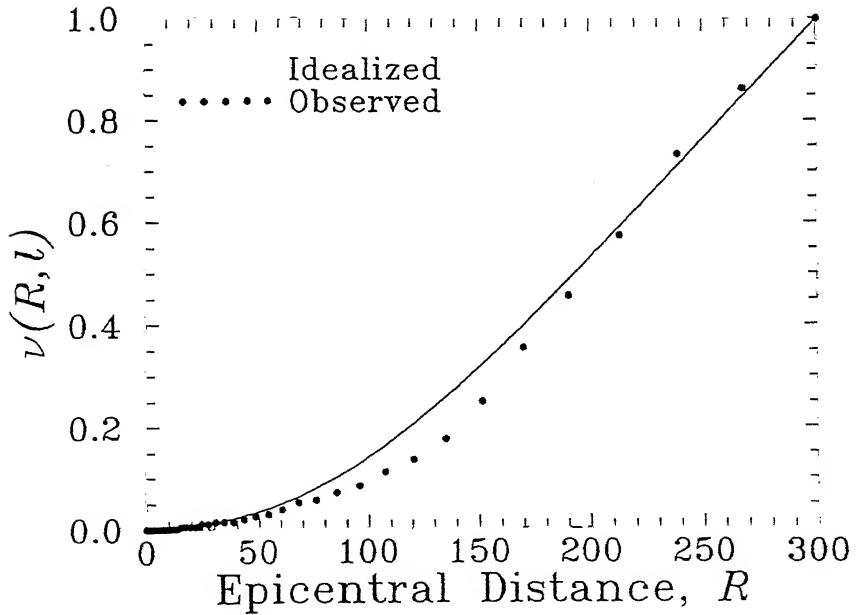
Figure 3.3 Cumulative Spatial Distributions of Earthquake Occurrences.

same proportions as are the past earthquake events with their epicenters in these source elements. To determine these proportions, a cumulative distribution plot of the actual earthquake occurrences within the 50 source elements, as normalized to a maximum value of unity, is prepared. A plot of such a distribution for the grid point with 24.1° latitude and 93.1° longitude is shown in Fig. 3.3 along with its idealized form. To know the number of earthquakes of magnitude, M_j (this implies $M_j \pm 0.2$ with $\delta M = 0.4$), likely to occur in Y years within a distance, R, from a site, l, one has to first find out the ordinate of idealized distribution plot corresponding to R, say $\nu(R, l)$, and then multiply this with $N(M_j)Y$. The expected number of earthquake events of magnitude M_j in case of the ith source element will then be

$$n_i(M_j) = [\nu(R_i, l) - \nu(R_{i-1}, l)] N(M_j) Y \qquad (3.4)$$

For this study, Y will be taken as 100 years.

CHAPTER IV

UNIFORM HAZARD MAPS FOR NORTH-EAST INDIA

4.1 Introduction

In probabilistic seismic hazard analysis, construction of hazard maps based on uniform hazard spectrum (UHS) is the usual objective. The uniform hazard spectrum can be defined as a spectrum of any functional having the same probability of exceedance at each time-period over a specified duration. The functional can be any spectral property of ground motion, say, Fourier spectrum amplitude, PSA, PSV, etc. In the present study, the functional is considered to be PSA due to this being a popular design parameter. For this, UHS at various sites are first obtained for the PSV functional (due to the attenuation relationship having been developed for PSV in Chapter II) and then, those are converted to the UHS for PSA functional by multiplying with $2\pi/T$. The formulation for calculating UHS for PSV is first described briefly and then, contours for different (horizontal and vertical) PSA levels are drawn for 10 different SDOF oscillators of varying time-periods.

4.2 Review of Formulation for UHS

UHS for various sites are obtained by following a standard procedure given by Anderson and Trifunac (1977). Following is a brief review of this procedure for completeness in this study.

Let q_{ij} denotes the probability that a given PSV amplitude (at time-period, T) at a site will be exceeded during an event of size, M_j, taking place at

a source element, i. Eq. (2.10) can then be used to estimate $\epsilon(p, T)$ and thus, p ($= 1 - q_{ij}$) by using the residue-statistic plot in Fig. 2.2, with focal depth taken as in Appendix. The average focal depths of earthquake events vary with locations and this spatial variation is taken into account in the values given in Appendix. Assuming that earthquake events with magnitudes in the ($M_j - 0.2$, $M_j + 0.2$) range for the ith source element follow Poissonian distribution, $n_i(M_j)$ (see Eq. (3.4)) becomes the mean of this distribution. Thus, the probability of exactly k events to occur is

$$p_{ij}(k) = \frac{e^{-n_i(M_j)}[n_i(M_j)]^k}{k!} \tag{4.1}$$

Since $1 - (1 - q_{ij})^k$ represents the probability that during at least one of the k events, $PSV(T)$ will be exceeded, the probability that at least one event will cause $PSV(T)$ to be exceeded, becomes

$$P_{ij} = \sum_{k=0}^{\infty} [(1 - q_{ij})^k] \frac{e^{-n_i(M_j)}[n_i(M_j)]^k}{k!}$$
$$= 1 - \exp[-n_i(M_j)q_{ij}] \tag{4.2}$$

Now, considering all earthquake events that may occur in the entire circular zone around a site, the probability that $PSV(T)$ will be exceeded at the site in a period of Y years can be expressed as

$$p[PSV(T)] = 1 - \prod_{i=1}^{I} \prod_{j=1}^{J} (1 - P_{ij})$$

where I = total number of sites (which is same as the total number of grid points), and J = total number of source elements considered for each site. Using Eq. (4.2), this is simplified to

$$p[PSV(T)] = 1 - \exp\left[-\sum_{i=1}^{I}\sum_{j=1}^{J} q_{ij}n_i(M_j)\right] \tag{4.3}$$

Fig. 4.1 shows the cumulative probability distribution based on this relationship for $T = 0.04$, 0.12 and 0.50 s in case of the horizontal component at grid point having 23.6° latitude and 91.4° longitude. When $p[PSV(T)]$ is known for several time-periods, a uniform hazard spectrum curve can be obtained for a given probability of exceedance, p. Fig. 4.2 shows plots of the (5% damping) UHS for $PSA(T)$ in case of horizontal and vertical motions, as obtained for $p = 0.5$ in case of the grid point having 24.5° latitude and 94.4° longitude.

4.3 Uniform Hazard Maps

Once UHS are known for all grid points, seismic hazard maps are obtained in terms of 5% damping PSA (in g) contours for a period of next 100 years. A total of twenty such hazard maps are shown in Figs. 4.3 to 4.22 corresponding to $T = 0.04$, 0.06, 0.08, 0.12, 0.17, 0.24, 0.34, 0.48, 0.70 and 1.0 s for $p = 0.50$, and for the horizontal and vertical components of ground motion. In each of the maps, vertical ordinate shows the latitude (in degree) while the horizontal ordinate represents the longitude (in degree) of a location.

From the hazard maps shown in Figs. 4.3 to 4.22, a general pattern consistent with some of the geological characteristics of the region is quite obvious. The contours passings through Manipur and Mizoram are parallel to the folded belt of Tripura and western part of Arakan Yoma (see seismotectonic map of the North-East India region in Fig. 4.23). The Naga Hills, having a north-east to south-west strike, comprise of several overthrust sheets. The contours in that area are parallel to that strike and the values decrease as one goes away, thus indicating Naga Hills as one of the potential sources of seismicity. A high value of
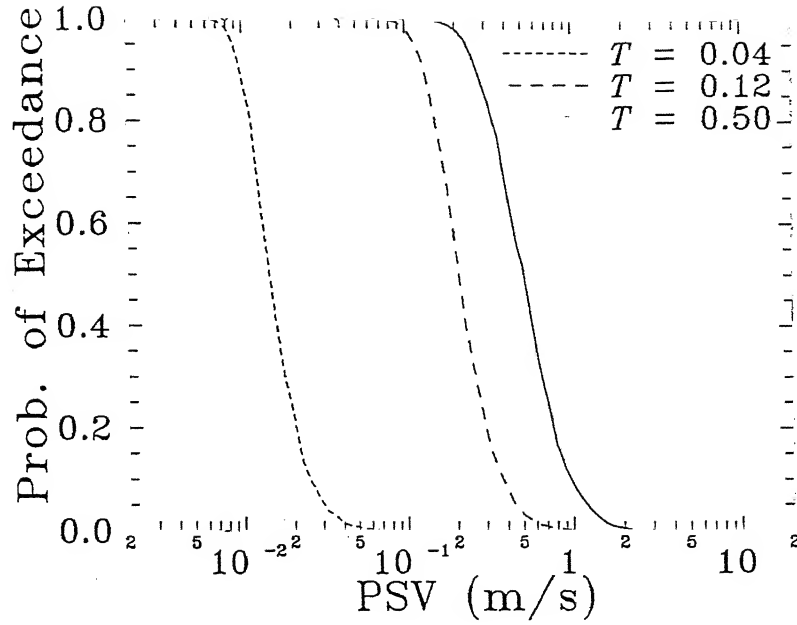
Figure 4.1 Cumulative Probability Distributions for PSV Amplitudes at Different Time-Periods.

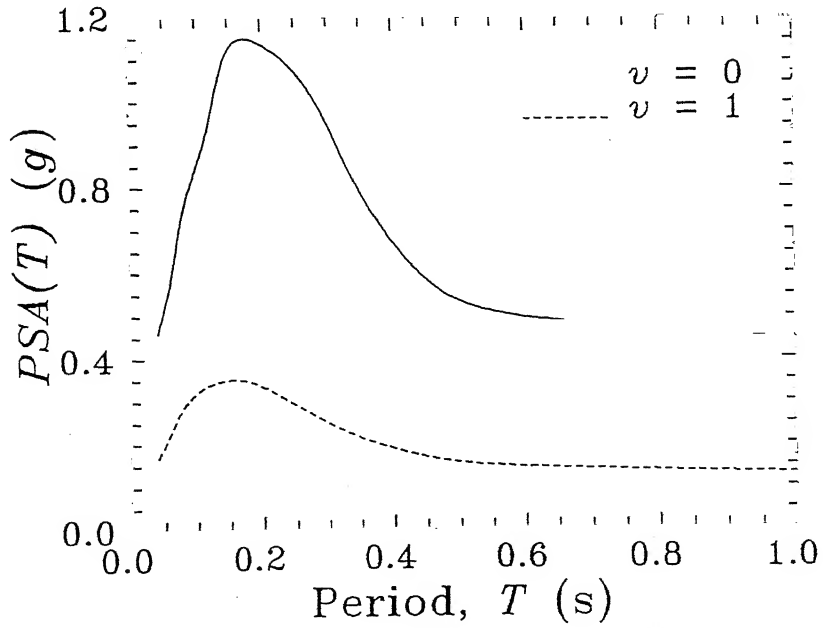**Figure 4.2** Uniform Hazard Spectra for Horizontal PSA ($v = 0$) and Vertical PSA ($v = 1$).

hazard level in the western part of Arunachal Pradesh reflects the fact that lots of earthquakes have taken place close to that region. In view of these observations, the objective model of seismicity adopted in this study appears to be acceptable for the North-East region, even though this is not based on identification of actual source zones of the region.

It may be mentioned that the proposed hazard maps are specifically for the stiff soil/rock sites due to the data used in the development of underlying attenuation model. Thus, the information available from these maps may need further processing for use in case of medium to soft soil deposits at a site.

4.4 Comparison with IS Code

It may be observed in any of the hazard maps for horizontal motion (except that for $T = 1.0$ s) that the difference between the minimum and maximum hazard levels is about 40% of the minimum level. Considering that this difference between hazard levels from one zone to the next higher zone is about 50% as per the IS code (IS: 1893 (2002)), considering the entire North-East India in a single zone V with uniform seismicity may not be proper. Further, the peak codal value of horizontal spectral acceleration (SA) for zone V is $0.9g$ (corresponding to 50% probability of exceedance and 100 years period) for 5% damping which is close to the highest estimated value of $0.99g$ only near the western part of Arunachal Pradesh at $T = 0.17$ s (see Fig. 4.11). In fact, for most of the region, the estimated PSA values are much lower (say, by about 50%) than those specified by the code. Apparently, the codal values are inconsistent with the return period (of 144 years) corresponding to $p = 0.5$ and $Y = 100$ years. Considering that

it is a world-wide practice to consider the return period of 475 years, the PSA values have been re-estimated for $p = 0.1$ and $Y = 50$ years. Table 4.1 shows the predicted values of PSA along with those prescribed by the IS code for major towns of the North-East region, viz. Guwahati (GH), Itanagar (IT), Kohima (KH), Dibrugarh (DG), Shillong (SH), Silchar (SC), Imphal (IM), Aizawl (AZ), and Agartala (AG), in case of $T = 0.04$, 0.06, 0.08, 0.12, 0.17, 0.24, 0.34, 0.48, 0.70, and 1.0 s. It may be seen that the codal values are now close to the estimated values at several time-periods and most of the towns, even though there is an overestimation of hazard at Agartala by 114% for 0.48 s period structures on one extreme and there is an underestimation of the hazard at Imphal by 42% for 1.0 s period structures on the other extreme. The observed discrepancies (within these two extremes) between the codal and estimated values are due to the choice of a fixed spectral shape and due to specifying the same PGA value for the entire North-East region in the code. Whereas the use of fixed spectral shape causes the hazard levels to remain unchanged in the code up to $T = 0.5$ s (for rock sites) (the estimated PSA values start falling after $T = 0.24$ s), hazard levels consistent with zone V are specified uniformly at all sites due to using same PGA, even though the region has seismicity varying from somewhere between zone IV and zone V (say, at Agartala) to somewhere between zone V and (extrapolated) zone VI (say, at Imphal). It is thus obvious that seismic hazard levels adopted by IS: 1893 (2002) correspond to much higher levels than those mentioned in the introductory remarks of the code (for $p = 0.5$ and $Y = 100$ years), and that the period-independent zoning map with the reliance on an average shape of response spectrum is inadequate. It will be useful to make a similar comparison of the estimated and codal values (for $p = 0.1$ and $Y = 50$ years) in case of vertical

acceleration values also. Table 4.2 shows that the codal values are much higher than those predicted by the present study (1.1–4.0 times higher) in case of the major towns of the North-East region. Considering a ratio of 1/2 instead of 2/3 to estimate the vertical PSA values from the horizontal PSA values **can** reduce this gap to reasonable levels.
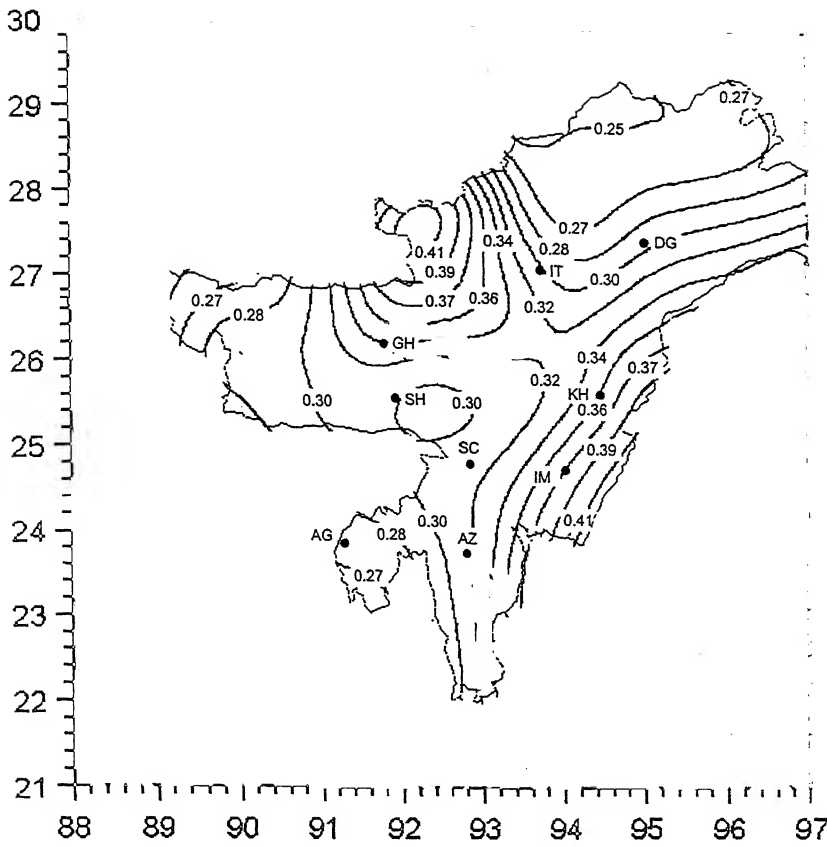
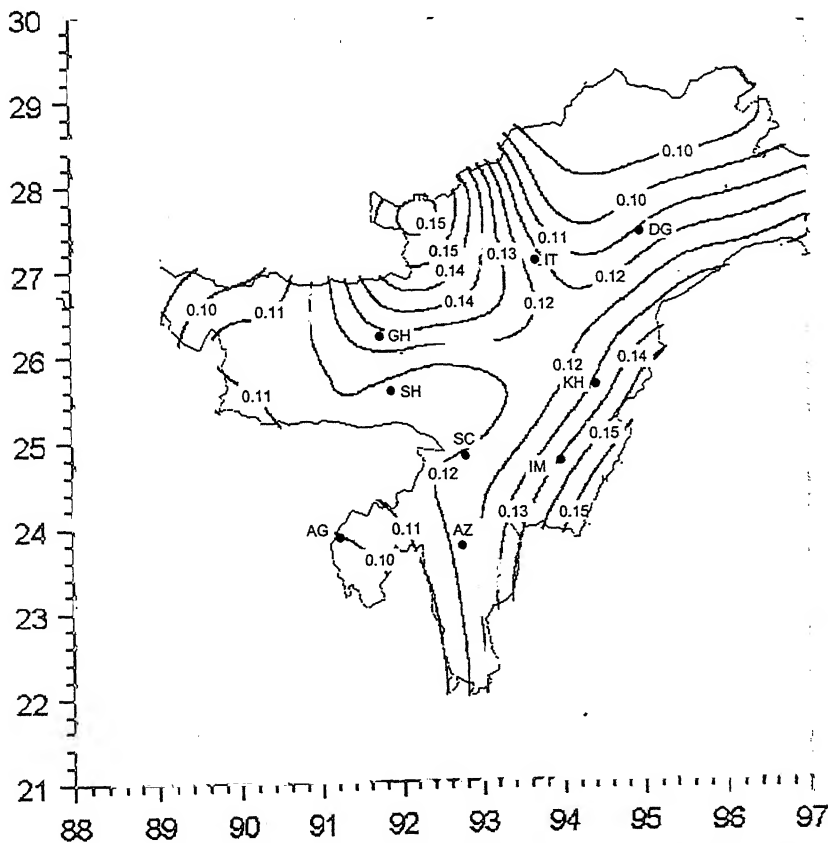**Figure 4.3** Map for Horizontal PSA in Case of $T = 0.04$ s.
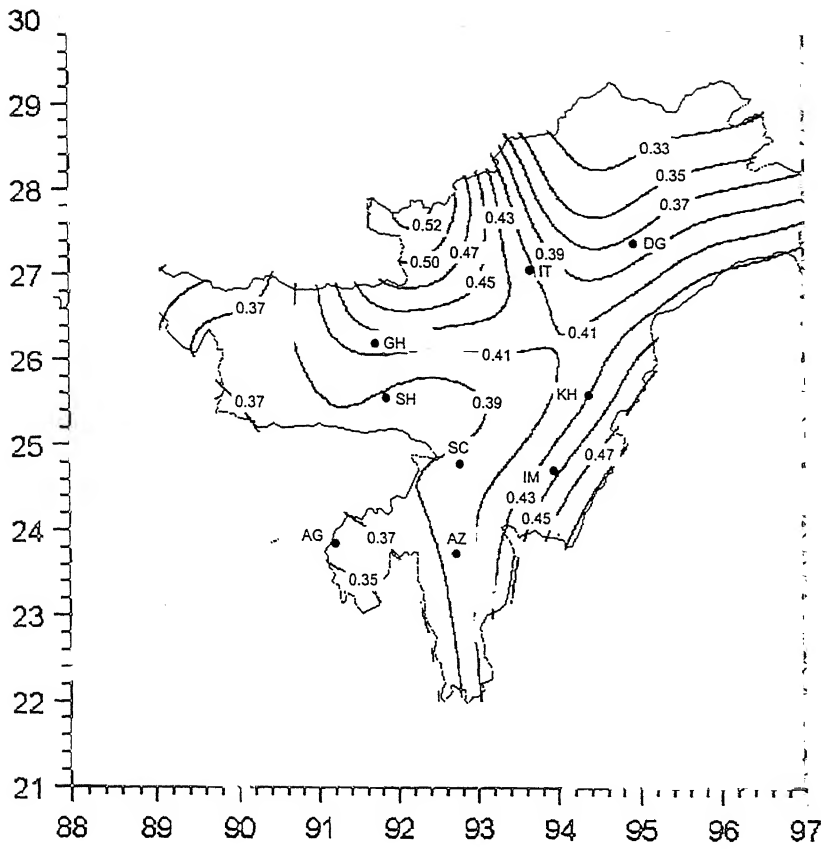

Figure 4.4 Map for Vertical PSA in Case of $T = 0.04$ s.

Figure 4.5 Map for Horizontal PSA in Case of $T = 0.06$ s.
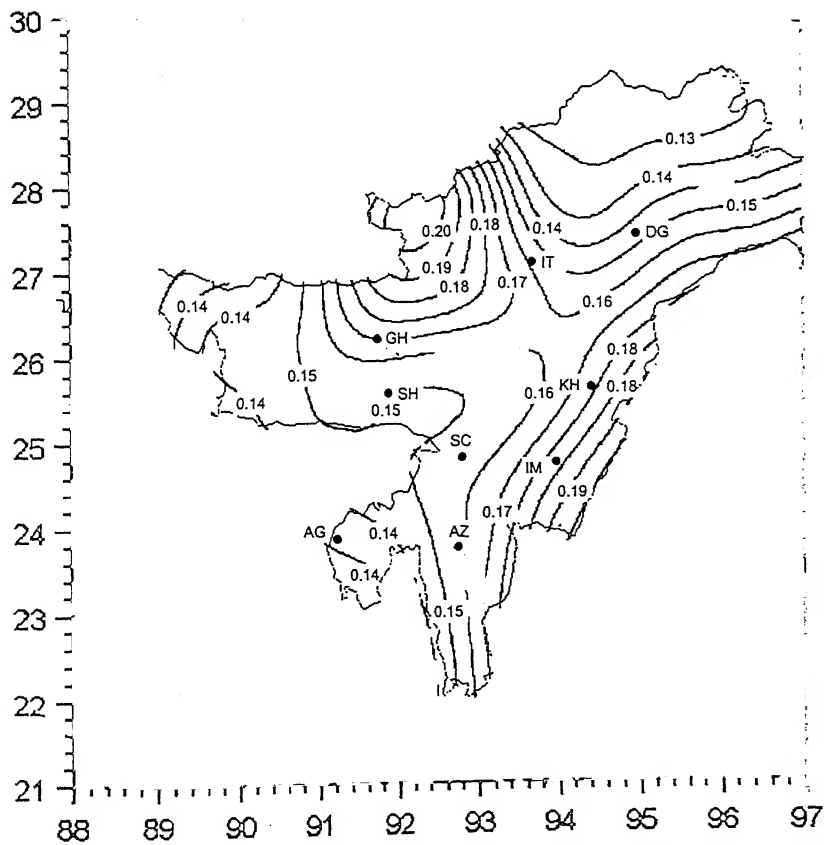
Figure 4.6 Map for Vertical PSA in Case of $T = 0.06$ s.
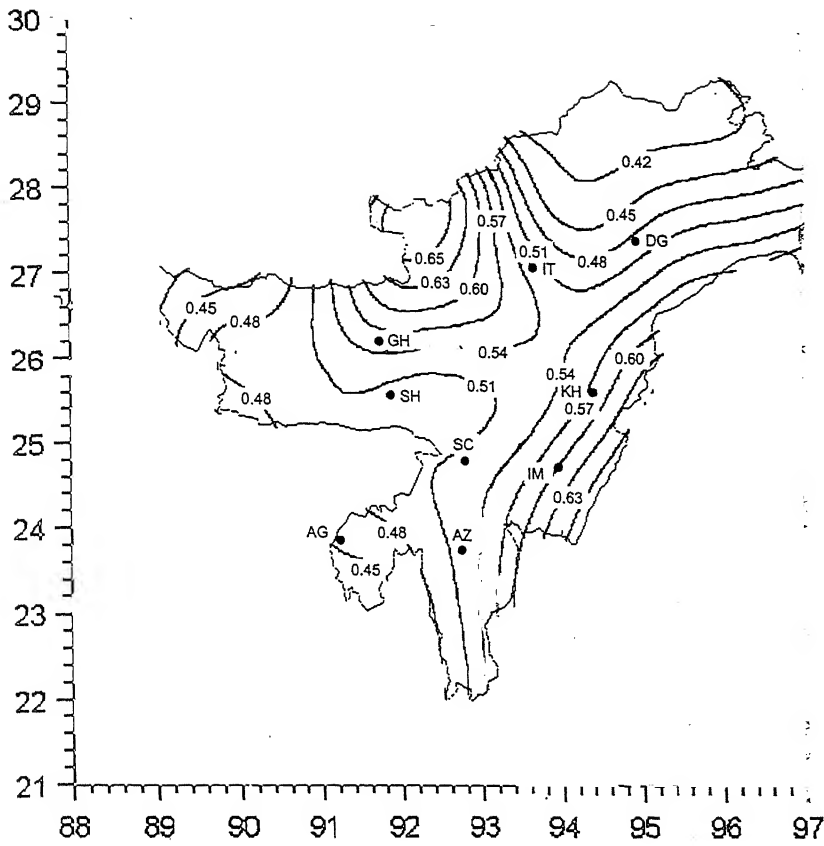
Figure 4.7 Map for Horizontal PSA in Case of $T = 0.08$ s.
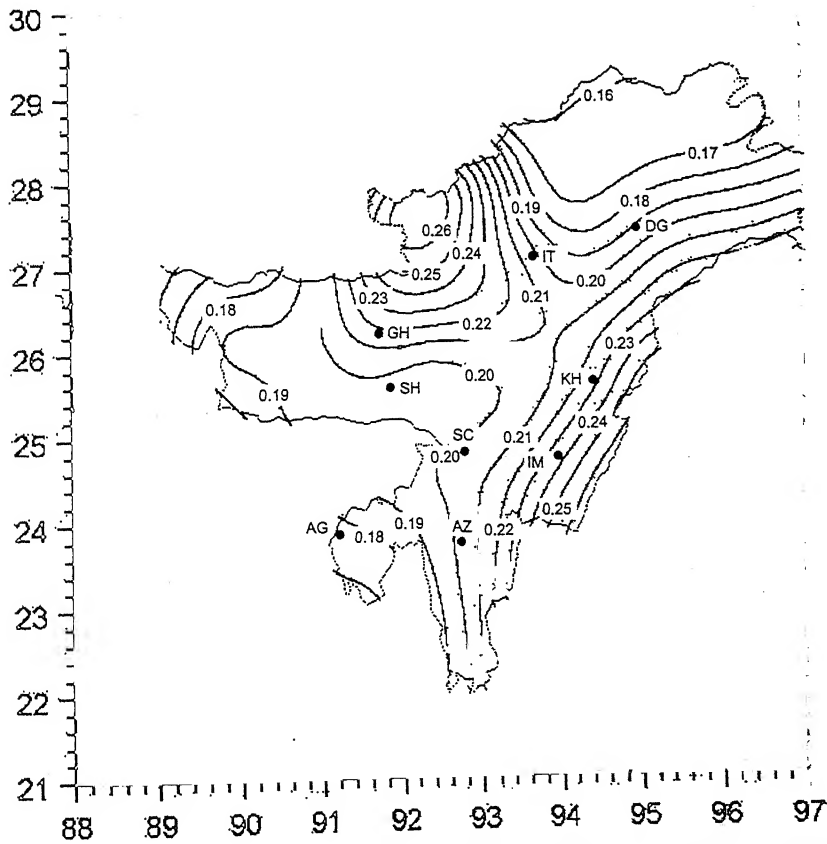
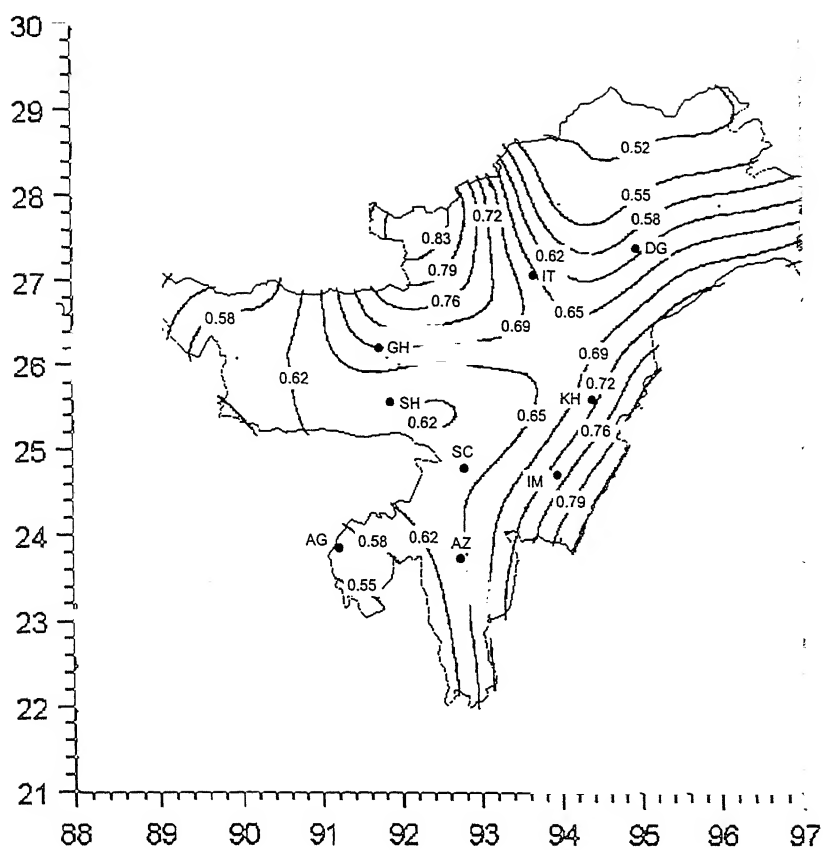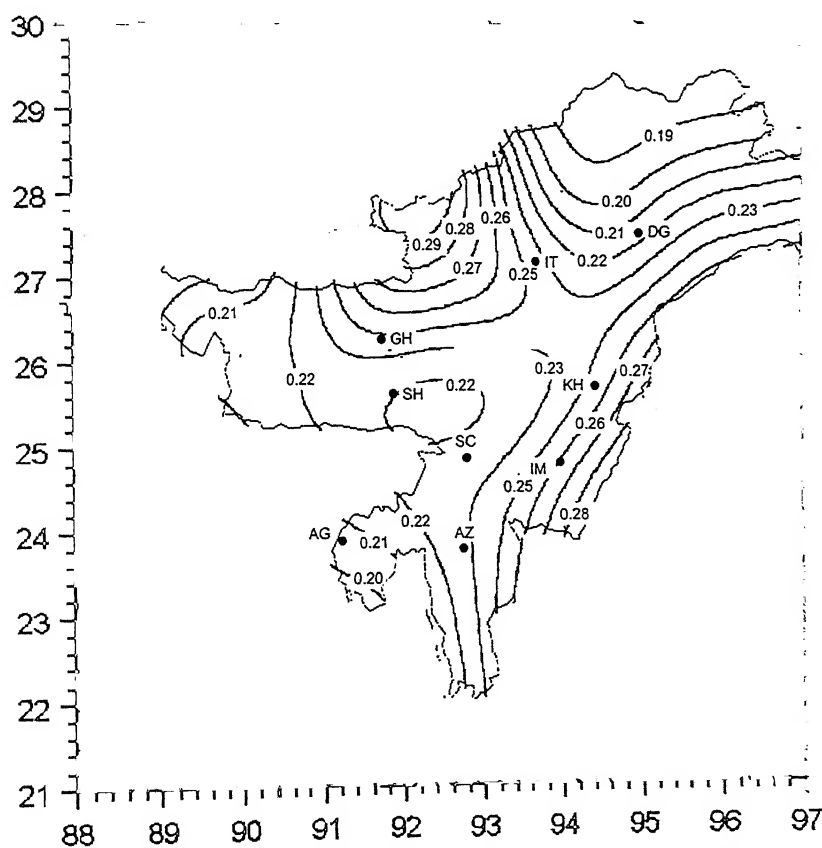**Figure 4.8** Map for Vertical PSA in Case of $T = 0.08$ s.

Figure 4.9 Map for Horizontal PSA in Case of $T = 0.12$ s.

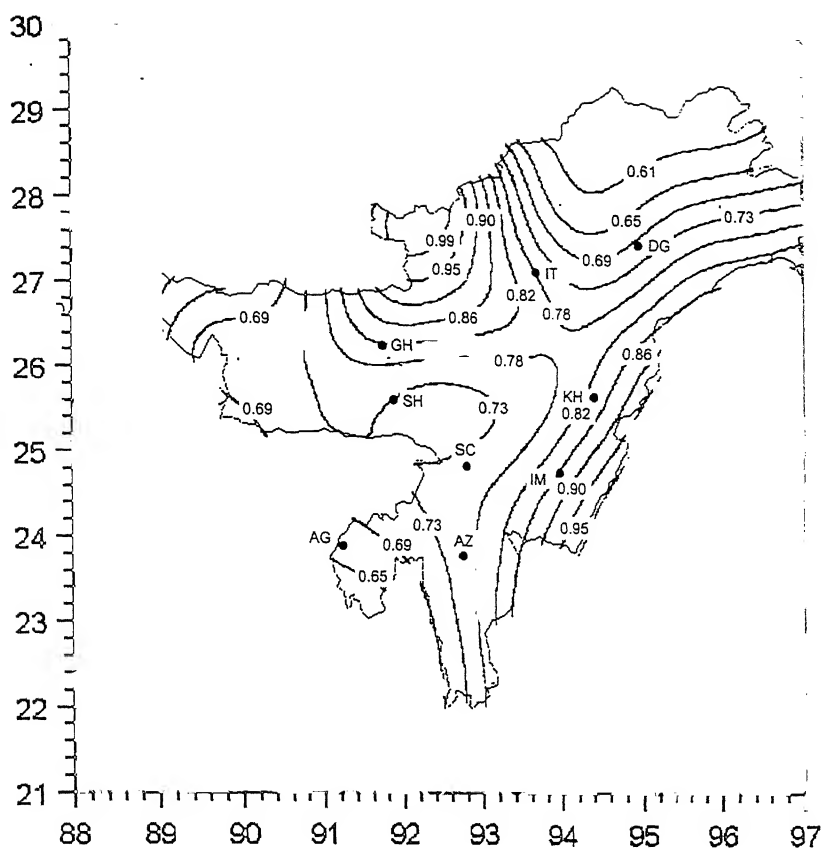**Figure 4.10** Map for Vertical PSA in Case of $T = 0.12$ s.

Figure 4.11 Map for Horizontal PSA in Case of $T = 0.17$ s.
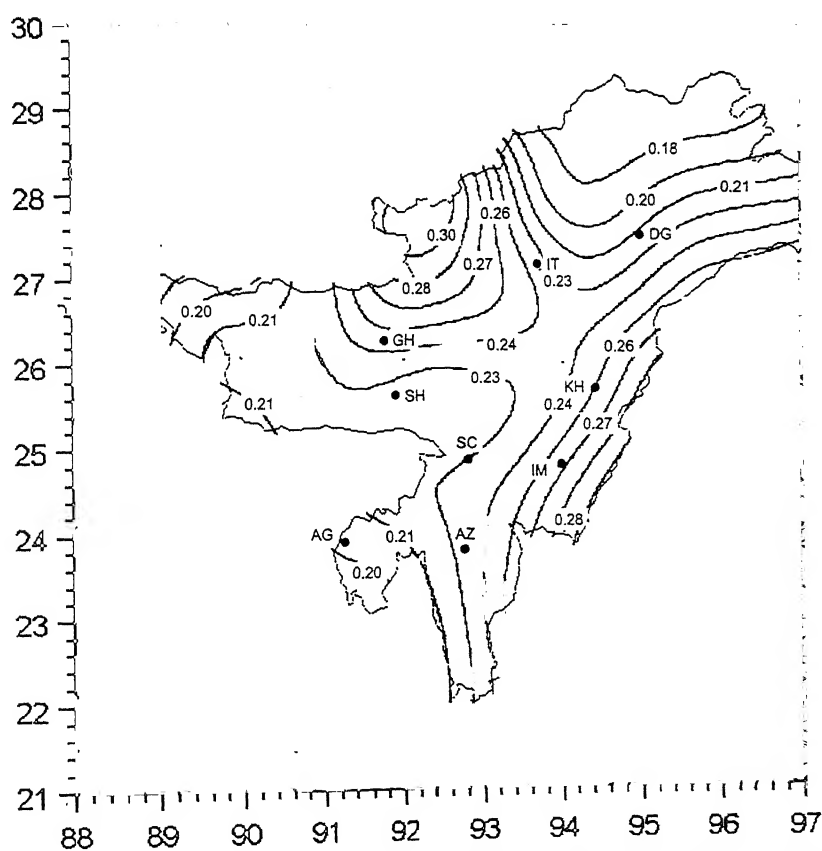

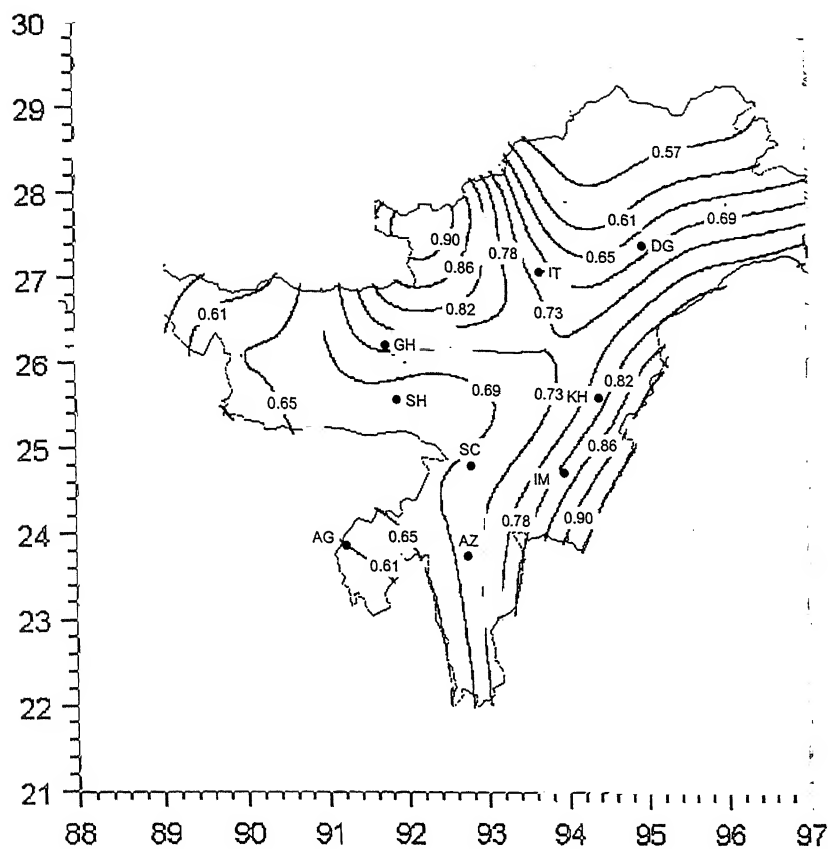Figure 4.12 Map for Vertical PSA in Case of $T = 0.17$ s.

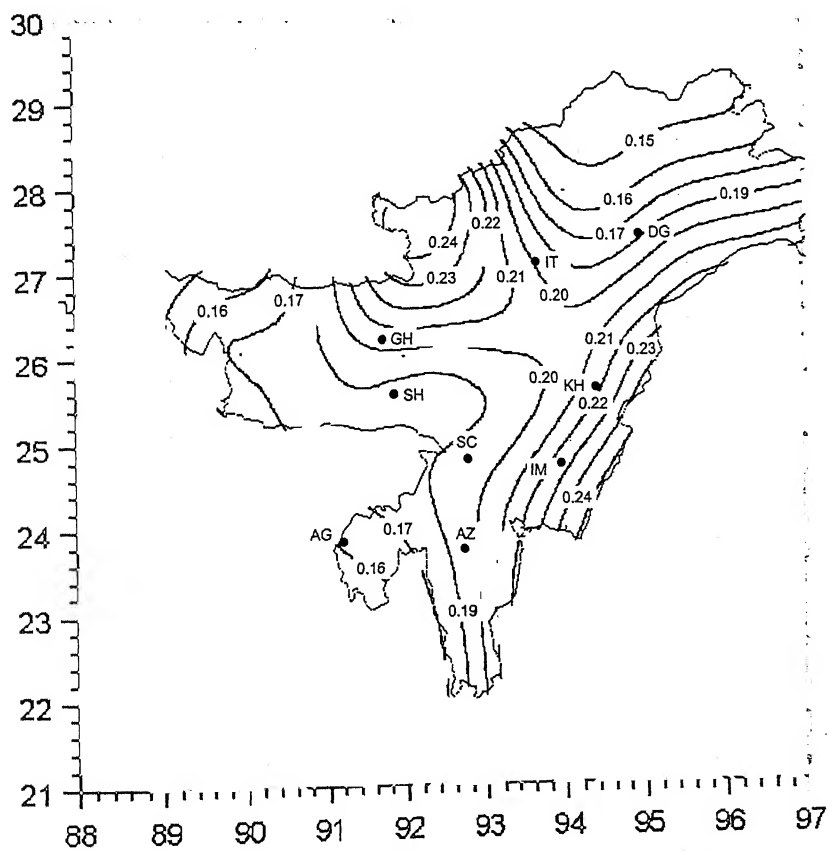Figure 4.13 Map for Horizontal PSA in Case of $T = 0.24$ s.

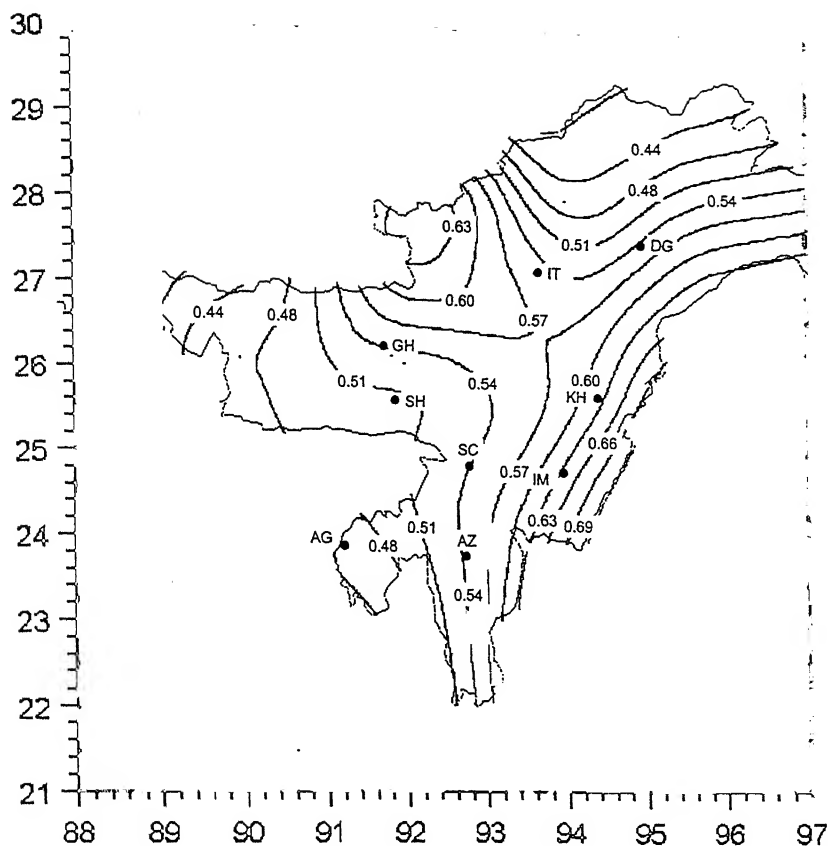Figure 4.14 Map for Vertical PSA in Case of $T = 0.24$ s.

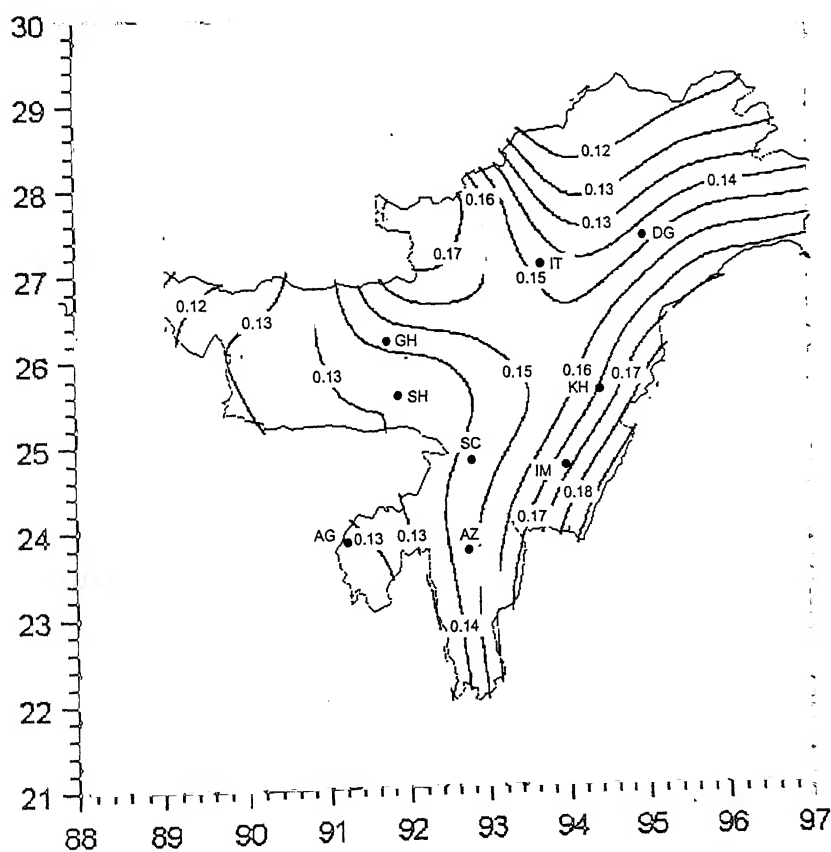**Figure 4.15** Map for Horizontal PSA in Case of $T = 0.34$ s.

Figure 4.16 Map for Vertical PSA in Case of $T = 0.34$ s.
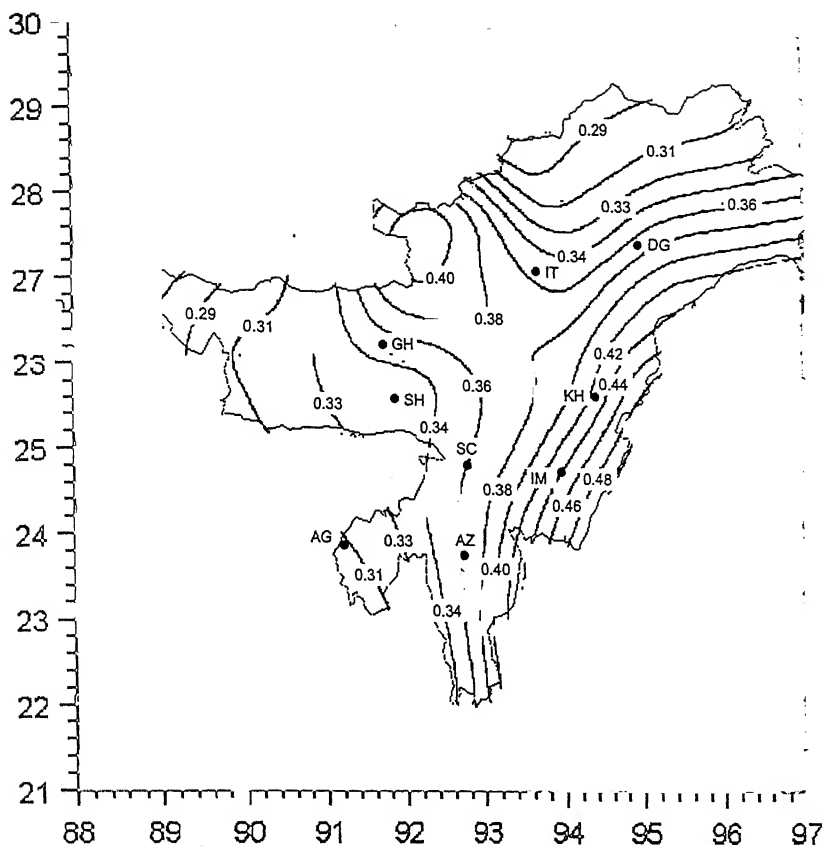
Figure 4.17 Map for Horizontal PSA in Case of $T = 0.48$ s.

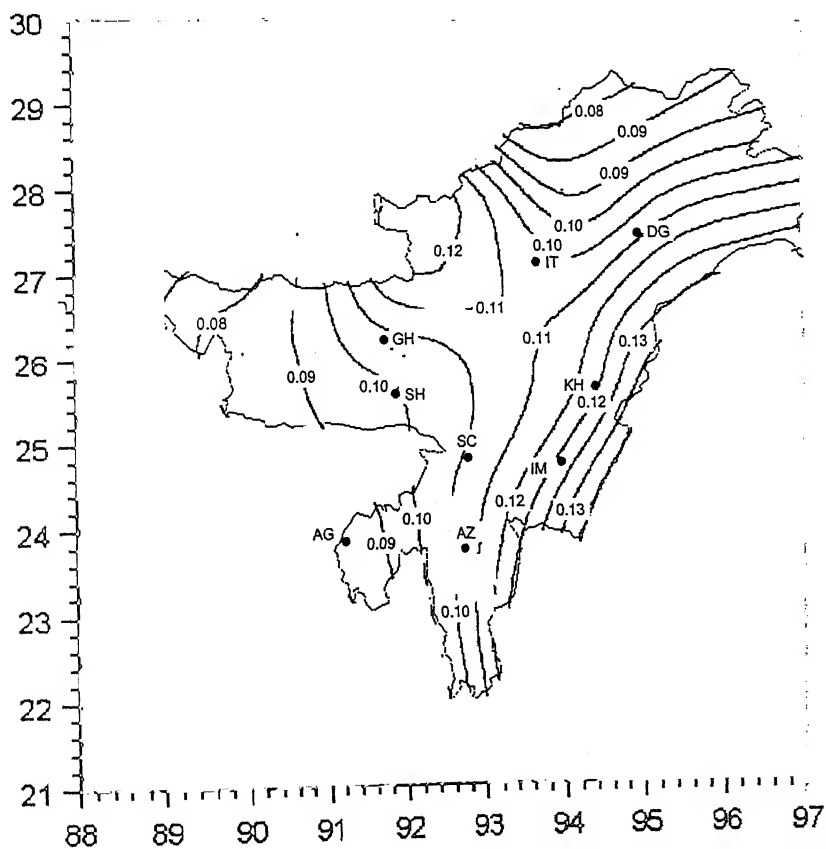

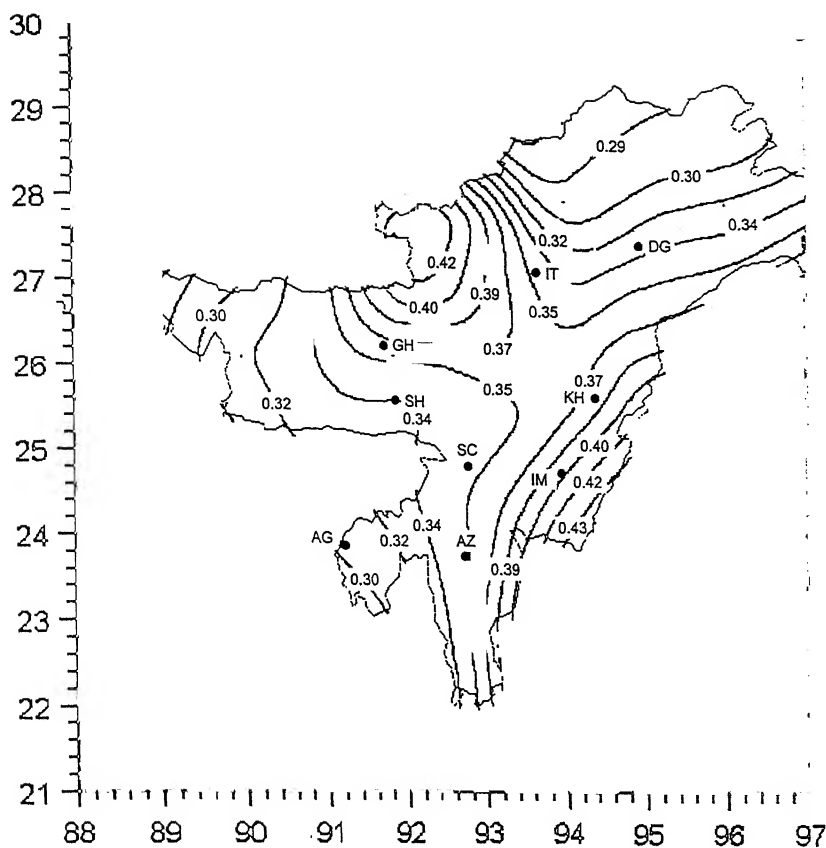**Figure 4.18** Map for Vertical PSA in Case of $T = 0.48$ s.

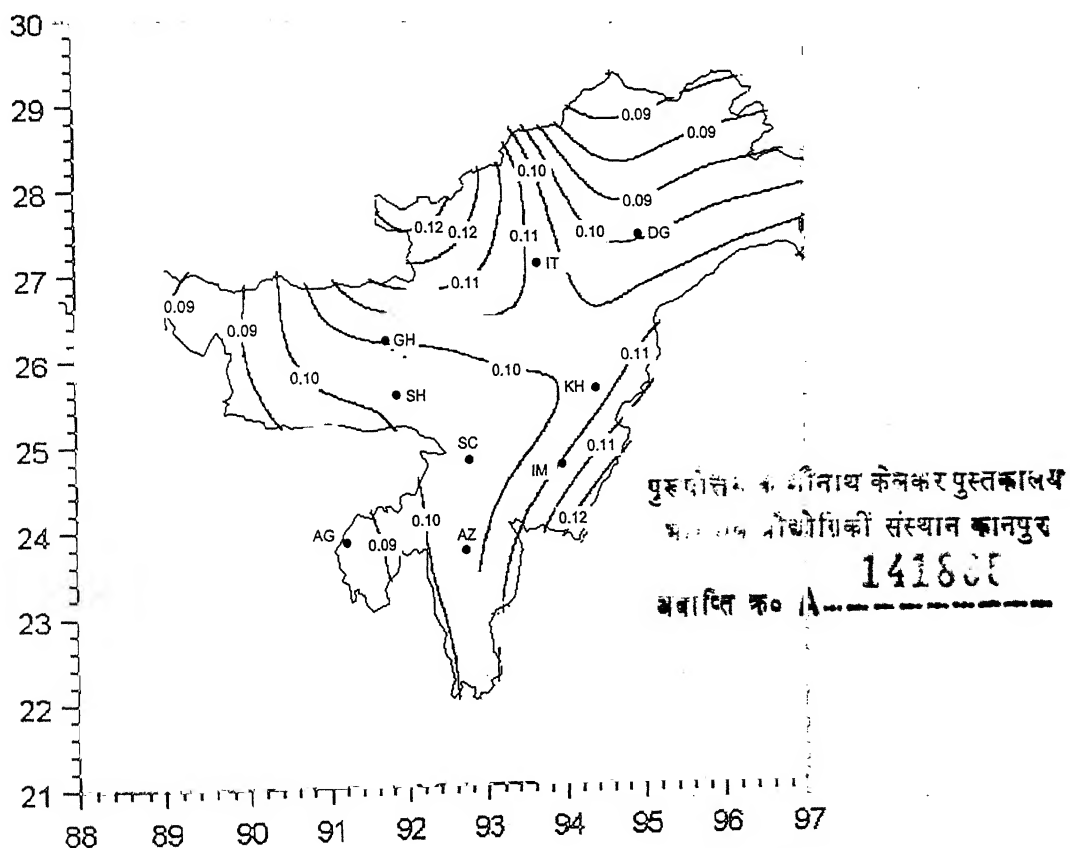**Figure 4.19** Map for Horizontal PSA in Case of $T = 0.70$ s.

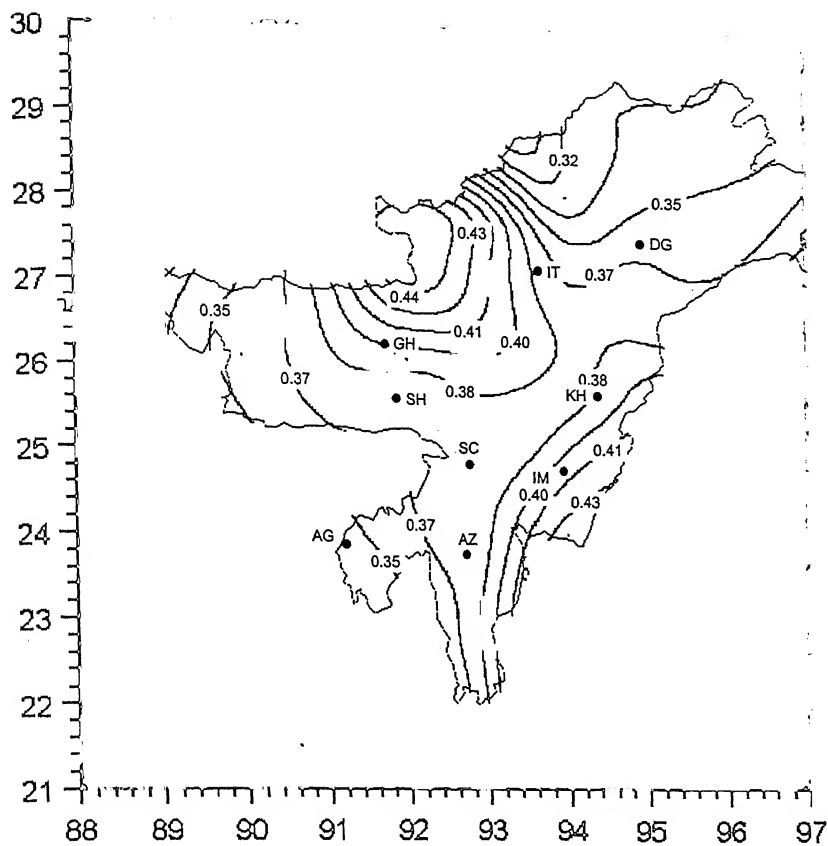**Figure 4.20** Map for Vertical PSA in Case of $T = 0.70$ s.

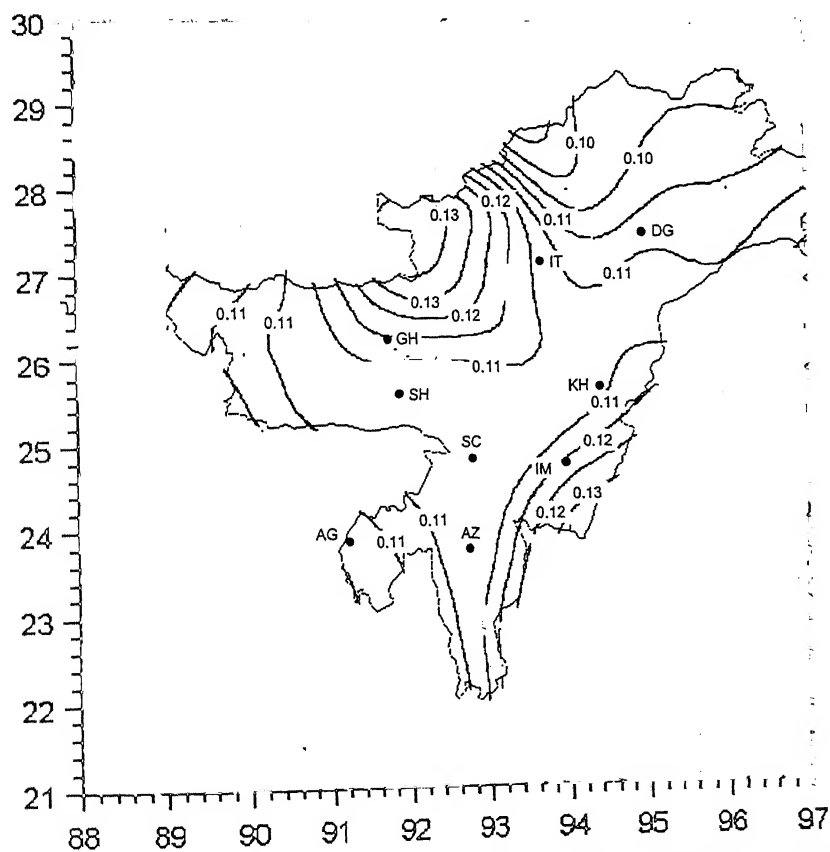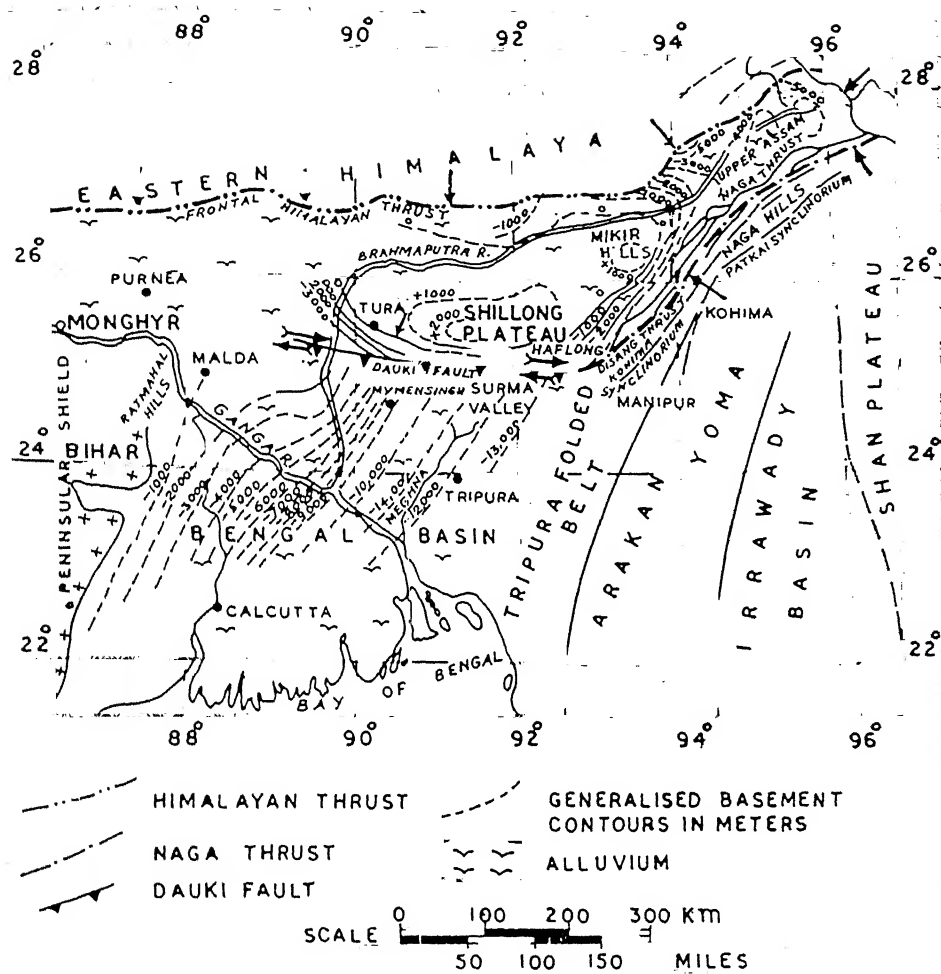**Figure 4.21** Map for Horizontal PSA in Case of $T = 1.0$ s.

Figure 4.22 Map for Vertical PSA in Case of $T = 1.0$ s.

Figure 4.23 Seismotectonic Map of North-East India (after Evans (1964)).

Table 4.1 - Comparison of Estimated and Codal PSA Values (in g) for Horizontal Component at Different Time Periods

Period, T (s)	Values from Present Study for p = 0.1 and Y = 50 years									Codal Value
	$\overline{G}H$	IT	KH	DG	SH	SC	IM	AZ	AG	
0.04	0.49	0.39	0.47	0.39	0.43	0.43	0.51	0.43	0.37	0.54
0.06	0.61	0.47	0.61	0.50	0.55	0.55	0.66	0.55	0.45	0.72
0.08	0.80	0.63	0.80	0.63	0.70	0.70	0.87	0.70	0.60	0.81
0.12	0.98	0.76	1.00	0.80	0.86	0.88	1.10	0.86	0.72	0.90
0.17	1.20	0.89	1.20	0.95	1.10	1.10	1.30	1.10	0.87	0.90
0.24	1.10	0.87	1.20	0.90	0.97	0.99	1.30	0.99	0.81	0.90
0.34	0.80	0.68	0.92	0.75	0.72	0.75	0.98	0.75	0.62	0.90
0.48	0.55	0.48	0.63	0.52	0.49	0.51	0.65	0.49	0.42	0.90
0.70	0.57	0.47	0.56	0.46	0.51	0.51	0.61	0.51	0.44	0.49
1.00	0.62	0.55	0.55	0.50	0.57	0.55	0.62	0.55	0.50	0.36

Abbreviations: GH - Guwahati, IT - Itanagar, KH - Kohima, DG - Dibrugarh, SH - Shillong, SC - Silchar, IM - Imphal, AZ - Aizwal, AG - Agartala

Table 4.2 - Comparison of Estimated and Codal PSA Values (in g) for Vertical Component at Different Time Periods

Period, T (s)	Values from Present Study for $p = 0.1$ and $Y = 50$ years									Codal Value
	GH	IT	KH	DG	SH	SC	IM	AZ	AG	
0.04	0.24	0.18	0.24	0.19	0.21	0.21	0.26	0.21	0.17	0.36
0.06	0.31	0.25	0.31	0.25	0.27	0.27	0.34	0.27	0.23	0.48
0.08	0.40	0.32	0.41	0.32	0.35	0.36	0.44	0.36	0.30	0.54
0.12	0.45	0.36	0.46	0.36	0.40	0.40	0.50	0.40	0.33	0.60
0.17	0.45	0.36	0.47	0.35	0.40	0.41	0.52	0.41	0.33	0.60
0.24	0.38	0.30	0.41	0.32	0.33	0.34	0.44	0.34	0.28	0.60
0.34	0.27	0.23	0.31	0.25	0.24	0.26	0.34	0.26	0.20	0.60
0.48	0.19	0.17	0.23	0.19	0.17	0.19	0.24	0.19	0.15	0.60
0.70	0.19	0.17	0.20	0.17	0.18	0.19	0.22	0.18	0.16	0.33
1.00	0.22	0.20	0.21	0.19	0.21	0.21	0.22	0.20	0.18	0.24

Abbreviations: GH - Guwahati, IT - Itanagar, KH - Kohima, DG - Dibrugarh, SH - Shillong, SC - Silchar, IM - Imphal, AZ - Aizwal, AG - Agartala

CHAPTER V
CONCLUSIONS

A probabilistic seismic hazard analysis based on the uniform hazard spectra for PSV has been carried out in North-East India. For this purpose, a spectral attenuation model has been proposed by using a total of 261 accelerograms recorded at different stations on stiff soil/rock sites in this region. The proposed model nicely captures the frequency-dependent variations in PSV for selected recorded motions and properly accounts for known effects of earthquake magnitude, epicentral distance and focal depth on the PSV spectral shape for both horizontal and vertical motions. An objective approach has been then attempted to define the seismicity model of the region of interest. This approach is based on the data for a large number of past earthquake events over a long period of time. In this approach, the entire region is divided into a fine grid of around 2500 nodes, and hazard level is predicted for each of the nodes by assuming it to be disturbed by the earthquake events within a 300 km distance. The numbers of events expected to occur in different magnitude classes are obtained from G-R relationship conforming to the data of past earthquake events. These are then distributed over 50 source elements, with each source element assumed to be representing an annular-shaped area around the node of interest. Even though actual source zones are not indentified in this approach, the estimated hazard mapping is found to be consistent with the seismotectonics and seismicity of the North-East region.

Seismic hazard maps for 50% probability of confidence and ten periods

have been proposed in terms of 5% damping PSA contours. These maps provide much more detailed and direct information about the seismic hazard than those based on the use of PGA together with a standard spectral shape. These maps may however require modifications for medium and soft soil conditions due to possible local amplifications. A comparison of the proposed maps with the seismic hazard envisaged by IS: 1893 (2002) shows that the zoning map together with the spectral shape in the code corresponds to comparable levels of seismic hazard to those predicted by this study, provided the PGA values given in the code correspond to $p = 0.1$ and $Y = 50$ years instead of $p = 0.5$ and $Y = 100$ years (50% risk level and 100 years service life). It is also seen that the vertical PSA levels specified by the code are on the higher side for most sites of the North-East India and that it is unrealistic to describe the seismic hazard for structures of varying time-periods in the entire North-East India via a single UHS.

APPENDIX

SPATIAL VARIATION OF FOCAL DEPTH

In North-East India and its surrounding areas, focal depths of past earth-quake events have varied within a wide range. However, a spatial dependence of the average focal depth can still be observed within this region. Primarily based on this observation, the entire region is divided into several sub-regions having different average focal depths. Five vertical sections of different lengths are taken and the average focal depths are obtained from the focal depths of different earthquake events observed at these sections. These sections are oriented along straight lines in different directions as shown in Fig. A.1. The earthquakes that occured in the vicinity of these sections are projected on them, and at each of such sections, the average focal depths are calculated for different length segments along the section. The assumed five sections with projected events are shown in Figs. A.2 to A.6. The so-obtained average focal depths are classified in the categories of six focal depths: 10, 15, 20, 25, 50 and 100 km, for simplicity. The different sub-regions to which each of these depths applies are idealized as in Fig. A.7. It is noticeable that the adopted approximate procedure accounts for the spatial variation of focal depth, while reducing the complexity of calculation.
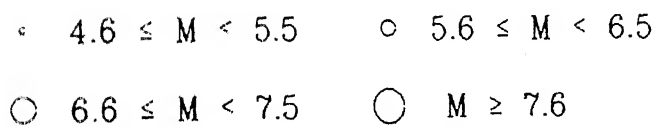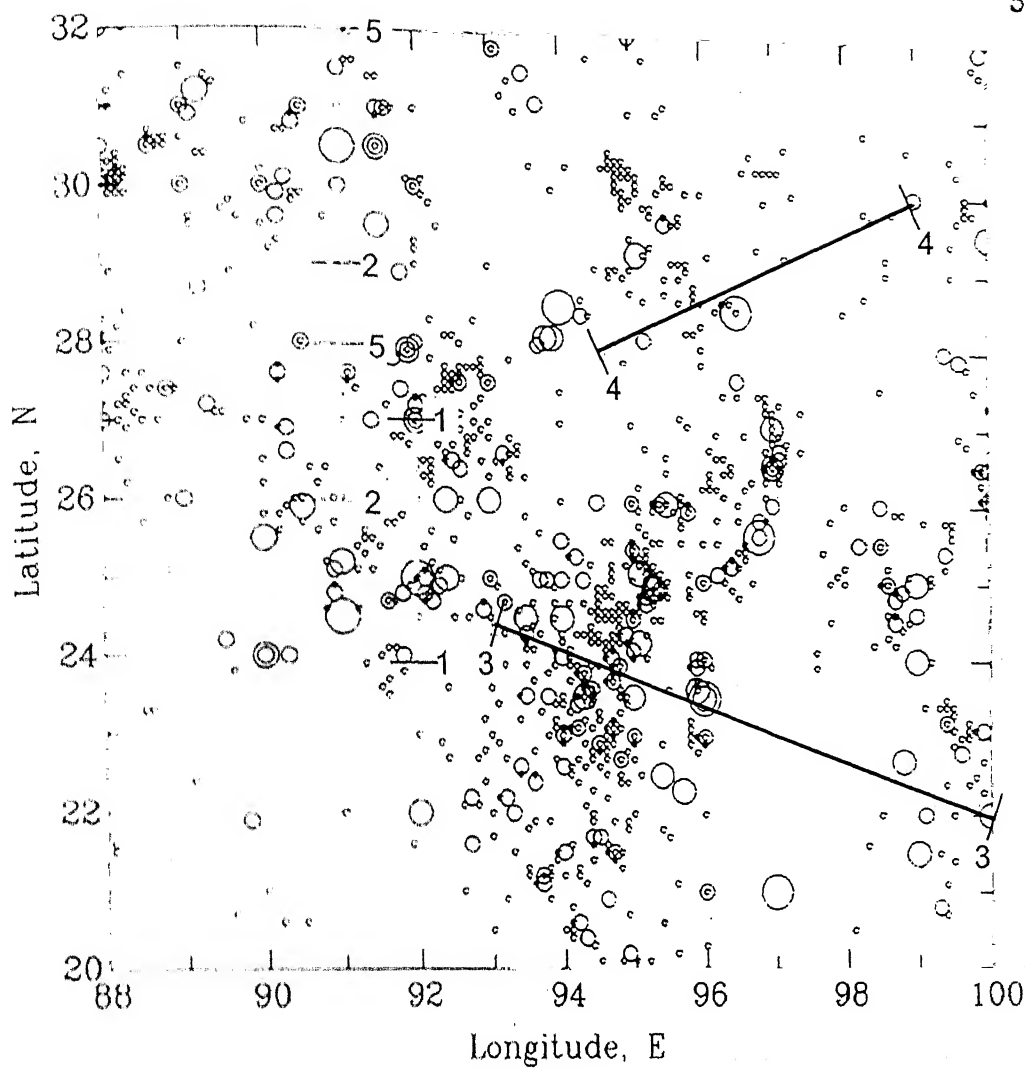
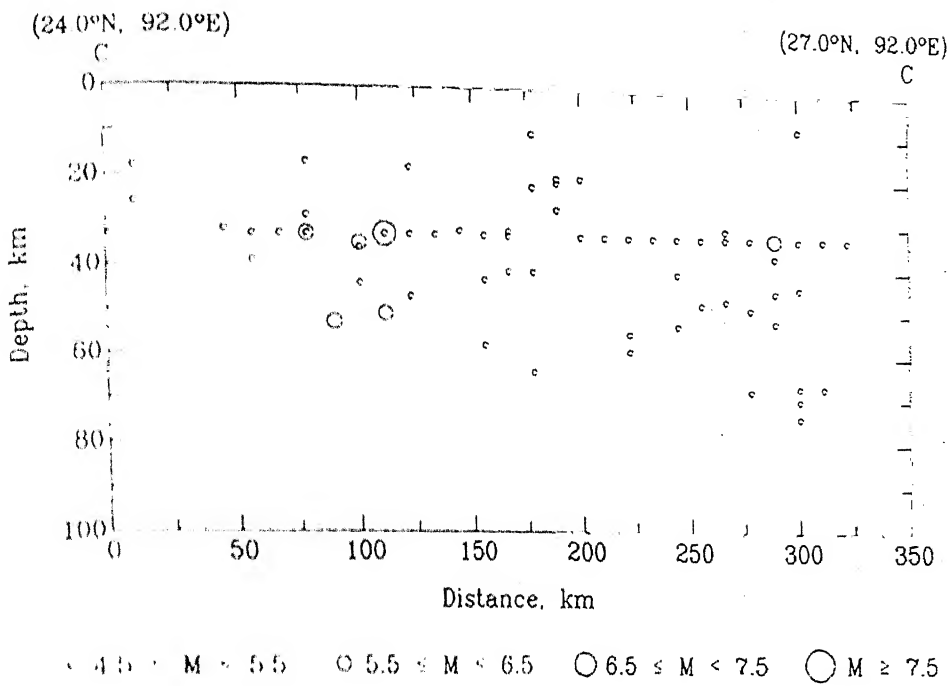Figure A.1 Traces of the Considered Vertical Sections.

Figure A.2 Vertical Section 1-1 with Projected Earthquake Events.
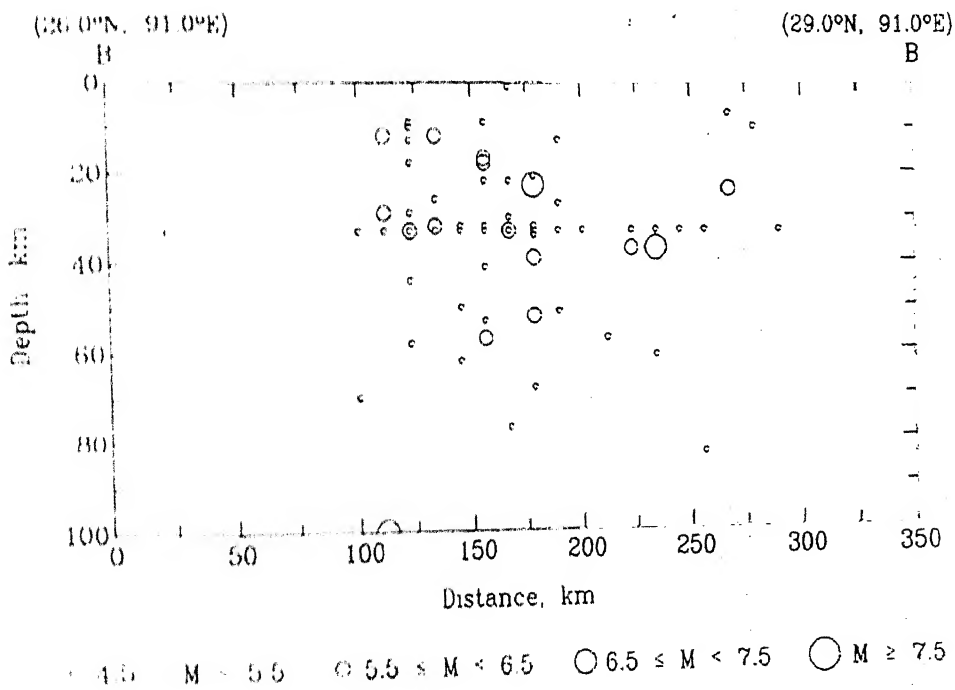

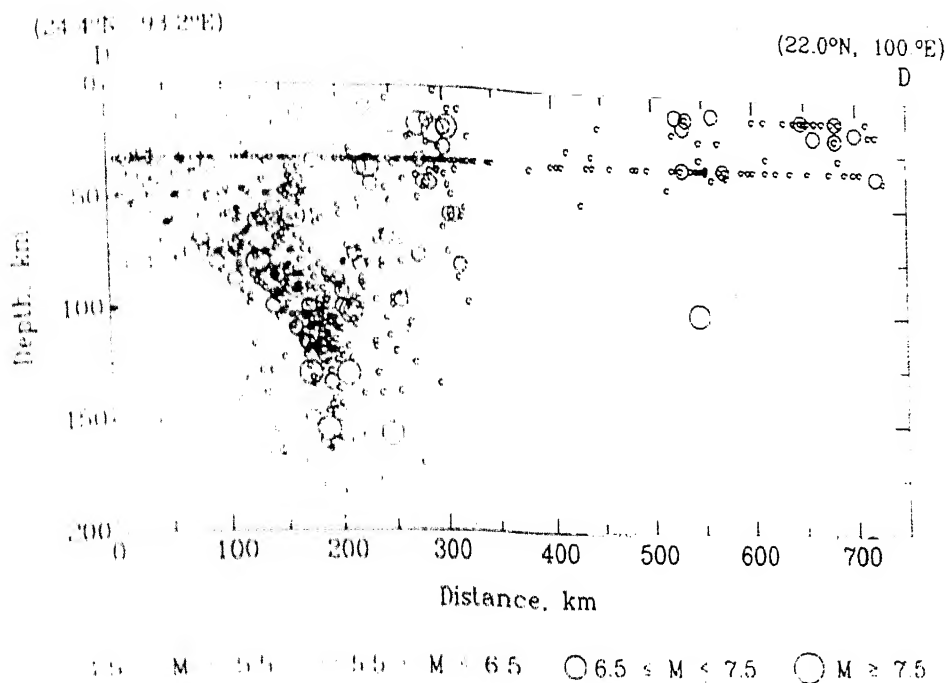**Figure A.3** Vertical Section 2-2 with Projected Earthquake Events.

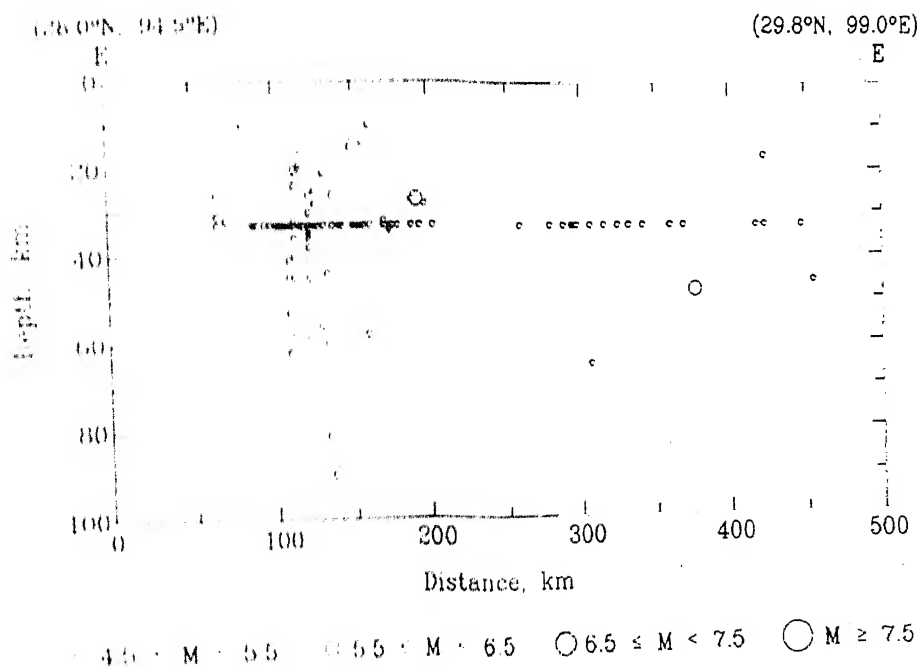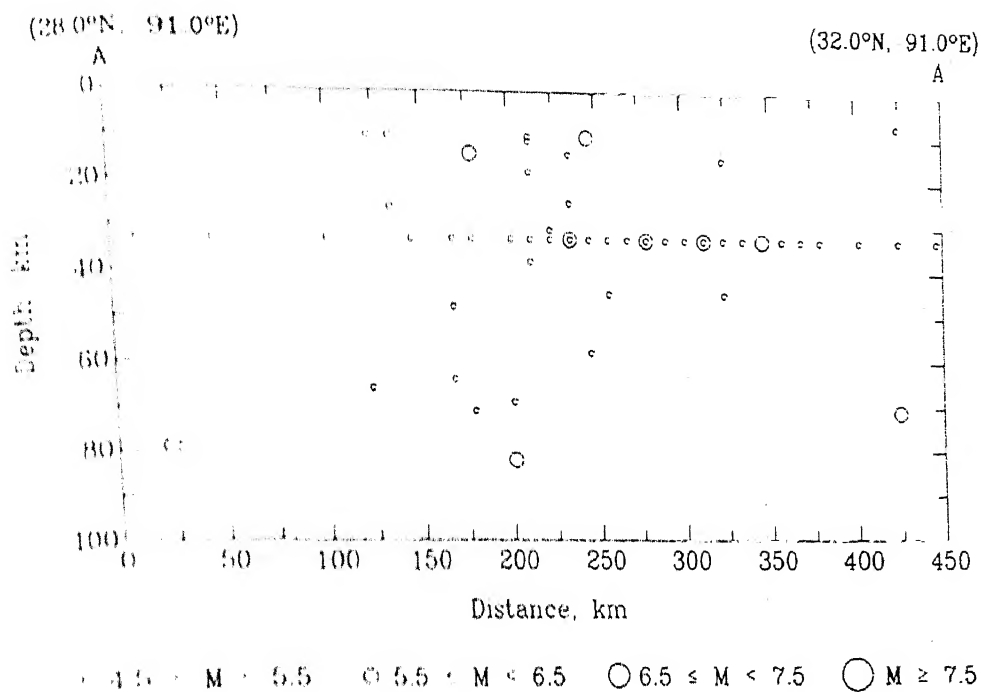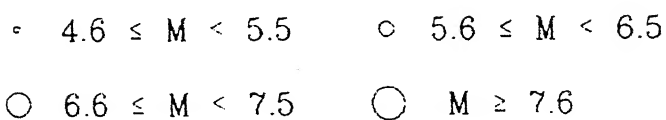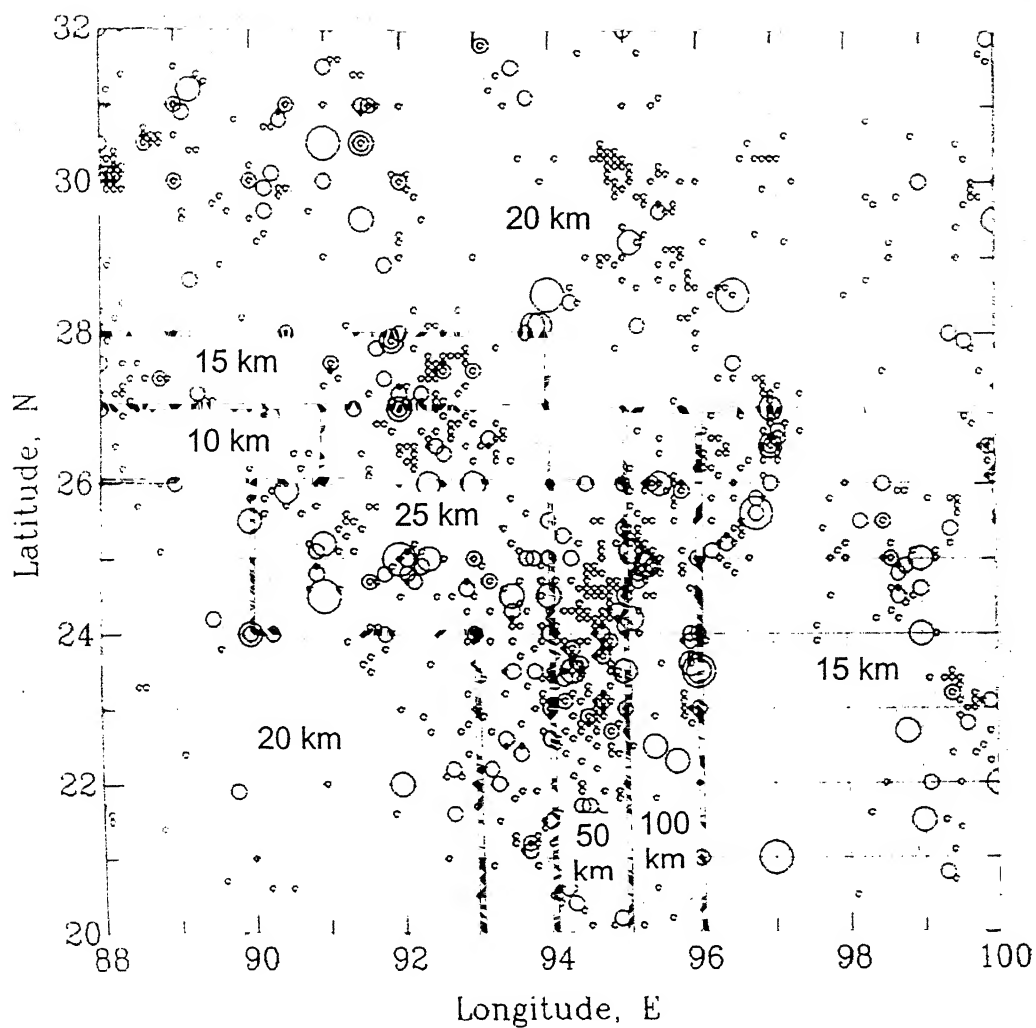**Figure A.4** Vertical Section 3–3 with Projected Earthquake Events.

Figure A.5 Vertical Section 4–4 with Projected Earthquake Events.

Figure A.6 Vertical Section 5-5 with Projected Earthquake Events.

Figure A.7 Idealized Sub-regions of Uniform Average Focal Depths.

REFERENCES

Anderson, J.G. (1997). Benefits of scenario ground motion maps, *Eng. Geology,* **48**, 43–57.

Anderson, J.G. and M.D. Trifunac (1977). On uniform risk functionals which describe strong earthquake ground motion: definition, numerical estimation, and an application to the Fourier amplitude of acceleration, *Report CE 77-02, University of Southern California, Los Angeles, California, U.S.A.*

Atkinson, G.M. (1990). A comparison of eastern North American ground motion observations with theoretical predictions, *Seism. Research Letters,* **61(3-4)**, 171–180.

Bommer, J.J., S.G. Scott, and S.K. Sarma (2000). Hazard-consistant earthquake scenarios, *Soil Dyn. Earthq. Eng.,* **19**, 219–231.

Boore, D.M., W.B. Joyner, and T.E. Fumal (1993). Estimation of response spectra and peak accelerations from western North American earthquakes: an interim report, *Open-File Report 93-509, U.S. Geological Survey, U.S.A.*

Chandler. A.M., L.S. Chan, and N.T.K. Lam (2001). Deterministic seismic hazard parameters and engineering risk implications for the Hong Kong region, *J. Asian Earth Sci.,* **20**, 59–72.

Chapman, M.C. (1999). On the use of elastic input energy for seismic hazard analysis, *Earthq. Spectra,* **15(4)**, 607–635.

Cornell, C.A. (1968). Engineering seismic risk analysis, *Bull. Seism. Soc. Amer.,* **58**, 1583–1606.

Cornell, C.A., H. Banon, and A.F. Shakal (1979). Seismic motion and response prediction alternatives, *Earthq. Eng. Struct. Dyn.,* **7(4)**, 295–315.

Crouse, C.B., Y.K. Vyas, and B.A. Schell (1988). Ground motions from subduction-zone earthquakes, *Bull. Seism. Soc. Amer.,* **78**, 1–25.

Dahle, A., H. Bungum, and L.B. Kvamme (1990). Attenuation models inferred from intraplate earthquake recordings, *Earthq. Eng. Struct. Dyn.,* **19**, 1125–1141.

Devillers, C. and B. Mohammadioun (1981). French methodology for determining site-adapted SMS (Séismic Majoré de Sécurité) spectra, *Trans. Sixth Int. Conf. Struct. Mech. Reactor Tech.,* **K(a)**, K-1/9.

Douglas, B.M. and A. Ryall (1975). Return periods for rock acceleration in western Nevada, *Bull. Seism. Soc. Amer.*, **65**, 1599–1611.

Evans, P. (1964). The tectonic framework of Assam, *J. Geological Soc. India*, **5**, 80–96.

Gupta, I.D. and T.V.S. Ramkrishna (1984). Evaluation of risk Fourier spectra for a site in Assam seismic gap, Northeast India, *Bull. Indian Soc. Earthq. Tech.*, **21(2)**, 62–72.

Gutenberg, B. and C.F. Richter (1942). Earthquake magnitude, intensity, energy, and acceleration, *Bull. Seism. Soc. Amer.*, **32**, 163–191.

IS: 1893 (2002). Criteria for earthquake resistant design of structures: general provisions and buildings (fifth revision), *Bureau of Indian Standards, New Delhi.*

Johnson, R.A. (1973). An earthquake spectrum prediction technique, *Bull. Seism. Soc. Amer.*, **63(4)**, 1255–1274.

Joyner, W.B. and T.E. Fumal (1984). Use of measured shear-wave velocity for predicting geologic site effects on strong ground motion, *Proc. Eighth World Conf. Earthq. Eng.*, **2**, 777–783.

Kayabali, K. (2002). Modeling of seismic hazard for Turkey using the recent neotectonic data, *Eng. Geology*, **63**, 221–232.

Kijko, A. and A.O. Öncel (2000). Probabilistic seismic hazard maps for the Japanese islands, *Soil Dyn. Earthq. Eng.*, **20**, 485–491.

Lee, V.W. (1993). Scaling PSV from earthquake magnitude, local soil, and geologic depth of sediments, *ASCE J. Geotech. Eng.* **119(1)**, 108–126.

Lee, V.W. (1995). Pseudo relative velocity spectra in former Yugoslavia, *Eur. Earthq. Eng.*, **9(1)**, 12–22.

Lee, V.W. and M. Manić (1994). Empirical scaling of response spectra in former Yugoslavia, *Proc. Tenth Eur. Conf. Earthq. Eng.*, **4**, 2567–2572.

Lindholm, C.D. and H. Bungum (2000). Probabilistic seismic hazard: a review of the seismological frame of reference with examples from Norway, *Soil Dyn. Earthq. Eng.*, **20**, 27–38.

McGarr, A. (1984). Scaling of ground motion parameters, state of stress, and focal depth, *J. Geophys. Research*, **89**, 6969–6979.

McGuire, R.K. (1978). Seismic ground motion parameter relations, *J. Geotech. Eng. Div., Proc. ASCE,* **104(GT4)**, 481–490.

McGuire, R.K. (2001). Deterministic versus probabilistic earthquake hazard and risks, *Soil Dyn. Earthq. Eng.,* **21**, 377–384.

McGuire, R.K., W.J. Silva, and R. Kenneally (2001). New seismic design spectra for nuclear power plants, *Nucl. Eng. Des.,* **203**, 249–257.

Milne, W.G. and A.G. Davenport (1969). Distribution of earthquake risk in Canada, *Bull. Seism. Soc. Amer.,* **59**, 729–754.

Musson, R.M.W. (2000). Intensity-based seismic risk assessment, *Soil Dyn. Earthq. Eng.,* **20**, 353–360.

Musson, R.M.W., P.C. Marrow, and P.W. Winter (1994). Attenuation of earthquake ground motion in the UK, *Technical Report AEA/CS/16422000 /ZJ745/004, AEA Technology Consultancy Services (SRD) and British Geological Survey, U.K.*

Niazi, M. and Y. Bozorgnia (1992). Behaviour of near-source vertical and horizontal response spectra at SMART-1 array, Taiwan, *Earthq. Eng. Struct. Dyn.,* **21**, 37–50.

Orozova, I.M. and P. Suhadolc (1999). A deterministic-probabilistic approach for seismic hazard assessment, *Tectonophysics,* **312**, 191–202.

Peruzza, L., D. Slejko, and P.L. Bragato (2000). The Umbria-Marche case: some suggestions for the Italian seismic zonation, *Soil Dyn. Earthq. Eng.,* **20**, 361–371.

Reiter, L. (1990). Earthquake hazard analysis, *Colombia University Press, New York, U.S.A.*

Romeo, R. and A. Prestininzi (2000). Probabilistic versus deterministic seismic hazard analysis: an integrated approach for siting problems, *Soil Dyn. Earthq. Eng.,* **20**, 75–84.

Sabetta, F. and A. Pugliese (1996). Estimation of response spectra and simulation of nonstationary earthquake ground motion, *Bull. Seism. Soc. Amer.,* **86(2)**, 337–352.

Sokolov, V., C.H. Loh, and K.L. Wen (2001). Site-dependent design input ground motion estimations for the Taipei area: a probabilistic approach, *Probabilistic Eng. Mech.,* **16**, 177–191.

Spudich, P., W.B. Joyner, A.G. Lindh, D.M. Boore, B.M. Margaris, and J.B. Fletcher (1999). SEA99: a revised ground motion model prediction relation for use in extensional tectonic regimes, *Bull. Seism. Soc. Amer.*, **89(5)**, 1156–1170.

Stepp, J.C. (1973). Analysis of completeness of the earthquake sample in the Puget Sound area, in 'Seismic Zoning' (editor: S.T. Harding), *Report ERL 267-ESL30, NOAA Tech, Boulder, Colorado, U.S.A.*

Tento, A., L. Franceschina, and A. Marcellini (1992). Expected ground motion evaluation for Italian sites, *Proc. Tenth World Conf. Earthq. Eng.*, **1**, 489–494.

Theodulidis, N.P. and B.C. Papazachos (1994). Dependence of strong ground motion on magnitude-distance, site geology and macroseismic intensity for shallow earthquakes in Greece: II — horizontal pseudovelocity, *Soil Dyn. Earthq. Eng.*, **13(5)**, 317–343.

Trifunac, M.D. (1978). Response spectra of earthquake ground motion, *J. Eng. Mech. Div., Proc. ASCE*, **104(EM5)**, 1081–1097.

Trifunac, M.D. (1980). Effects of site geology on amplitudes of strong motion, *Proc. Seventh World Conf. Earthq. Eng.*, **2**, 145–152.

Trifunac, M.D. (1989). Dependence of Fourier spectrum amplitudes of recorded strong earthquake accelerations on magnitude, local soil conditions, and on depth of sediments, *Earthq. Eng. Struct. Dyn.*, **18**, 999–1016.

Trifunac, M.D. (1992). Should peak acceleration be used to scale design spectrum amplitudes?, *Proc. Tenth World Conf. Earthq. Eng.*, **10**, 5817–5822.

Trifunac, M.D. and V.W. Lee (1989). Empirical models for scaling pseudo relative velocity spectra of strong earthquake accelerations in terms of magnitude, distance, site intensity and recording site conditions, *Soil Dyn. Earthq. Eng.*, **8(3)**, 126–144.

Veneziano, D., C.A. Cornell, and T. O'Hara (1984). Historic method for seismic hazard analysis, *Report NP-3438, Electrical Power Research Institute, Palo Alto, U.S.A.*

Verma, R.K., M. Mukhopadhyay, and M.S. Ahluwalia (1976). Seismicity, gravity, and tectonics of Northeast India and Northern Burma, *Bull. Seism. Soc. Amer.*, **66(5)**, 1683–1694.

Wheeler, R.L. and C.S. Mueller (2001). Central US earthquake catalog for hazard maps of Memphis, Tennessee, *Eng. Geology*, **62**, 19–29.

A

A141835